

M.Sc. Thesis
Master of Science in Engineering

DTU Electrical Engineering
Department of Electrical Engineering

Coordinated Voltage Control of Offshore Wind Power and Multi-Terminal DC Grid

Rafael Calpe Domens (s161341)

Supervised by: Shaojun Huang
Kongens Lyngby 2018



DTU Electrical Engineering
Department of Electrical Engineering
Technical University of Denmark

Ørsteds Plads
Building 348
2800 Kgs. Lyngby, Denmark

Tel: (+45) 45 25 38 00
elektro@elektro.dtu.dk
www.elektro.dtu.dk



Summary

In this master thesis a Model Predictive Control is implemented for wind farm voltage control purposes. Aiming at upgrading the voltage level at the POC bus while improving also the rest of bus voltages. This MPC is based on a optimisation problem including system dynamics along a time-horizon. Hence, taking the best control action for minimising voltage deviations along a series of predicted states of the network.

According to the voltage control state-of-the-art, this project can be sorted by the following topics. It is a centralised park level controller based on system state optimisation. Focusing on the voltage target is a time-horizon dependent control since some of its input information comes from estimated future information. Furthermore, it handles a series of technologies such as WTG-converters, OLTC transformers and HVDC-VSC. These are integrated and coordinated in several strategies under the same scenario. Thus, working as a benchmark for further development of offshore wind power projects.

Along this work the following concepts are covered. First, an efficient voltage sensitivity technique is addressed analytically. Later on, this sensitivity is in charge of quantifying voltage errors related to the predicted system states. Second, the optimisation problem is explained for each strategy covering each of the controlled devices. This minimisation integrates the decision variables associated with each technology, system measurements, system set-points, system dynamics (state space model) and so, the predicted voltage deviation related to those future dynamics. Moreover, operational constraints of each device and voltage boundaries are defined. All these concepts are integrated into an MPC Matlab algorithm. Third, this MPC controller is modelled in DIgSilent PowerFactory providing the input for the controlled network devices. Then, carrying out a dynamic simulation for testing the performance of each strategy and technology. Finally, an extra strategy is set for further coordination with external network devices. Then, trying to bring some benefits to another grid while keeping optimal performance within the wind farm.

Resumen

En este trabajo de fin de máster (TFM) un controlador de modelo predictivo (MPC) es implementado para el control de voltaje en un parque eólico. En primer lugar, se trata de mejorar el nivel del voltaje en el nodo POC mientras se consiga también una mejora en el resto de nodos del parque. Este controlador MPC se basa en un problema de optimización que incluye las dinámicas de la red eléctrica a lo largo de un periodo de tiempo. Así pues, tomando las mejores acciones de control para minimizar la desviación del voltaje a lo largo de una serie de estados estimados de la red.

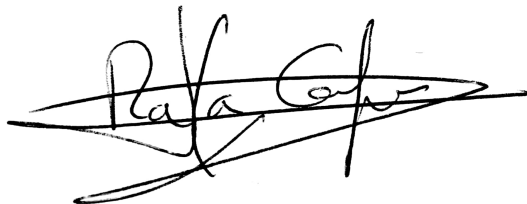
De acuerdo al actual estado del arte de controladores de voltaje, este proyecto se puede catalogar con los siguientes términos. Se trata de un controlador centralizado a nivel de parque basado en la optimización del estado del sistema. Mientras su objetivo principal es la reducción del error del voltaje, dicho controlador es dependiente del tiempo ya que incluye en sus decisiones información de estados futuros. Además, maneja y coordina una serie de tecnologías como las turbinas eólicas, transformadores y convertidores. Todos ellos integrados en diferentes estrategias y examinados bajo el mismo criterio. Por lo tanto, este proyecto pretende servir como referencia para futuros desarrollos y estudios en proyectos de energía eólica offshore.

A lo largo del proyecto se cubren los siguientes conceptos. Primero, una eficaz técnica para calcular analíticamente coeficientes de la sensibilidad del voltaje. Más tarde, estos coeficientes se encargan de cuantificar los errores del voltaje relacionados con los estados del sistema precedidos. En segundo lugar, un problema de optimización es explicado para cada una de las estrategias cubriendo cada uno de los dispositivos controlados. Dicha minimización integra las variables de decisión asociadas con cada tecnología, medición de la red, referencias del sistema y dinámicas del sistema. En tercer lugar, este controlador MPC es modelado en PowerFactory proporcionando la entrada para los dispositivos controlados en la red eléctrica. Posteriormente, cada tecnología y estrategia es evaluada mediante simulaciones dinámicas. Por último, una estrategia adicional es definida para aumentar la coordinación con dispositivos de una red externa al parque eólico. De esta forma, tratando de aportar mejoras a otra red mientras se conserva el funcionamiento óptimo dentro del parque.

Preface

This Master thesis was prepared at the department of Electrical Engineering at the Technical University of Denmark in fulfilment of the requirements for acquiring a Master of Science in Electrical Engineering, with study line in Electric Energy Systems.

Kongens Lyngby, February 27, 2018

A handwritten signature in black ink, appearing to read 'Rafael Calpe Domens', written over a horizontal line.

Rafael Calpe Domens (s161341)

Contents

Summary	i
Resumen	iii
Preface	v
Contents	vii
List of Figures	ix
List of Tables	x
Nomenclature	xi
1 Introduction	1
1.1 EU Future Objectives	1
1.2 New Power System Challenges	3
1.3 Grid Codes	4
1.4 Master Thesis' Objective	4
2 Voltage Control	7
2.1 Theoretical Principle	7
2.2 Literature review	8
2.3 Model Predictive Control	10
2.4 Sensitivity Coefficients	12
2.4.1 Sensitivity to Q Injections	13
2.4.2 Sensitivity to Slack Bus	13
2.4.3 Sensitivity to Tap Changes	14
2.4.4 Sensitivity Analysis Results	15
3 Wind Farm Coordination	19
3.1 Wind Farm Voltage Control	19
3.1.1 Optimisation	19
3.1.2 State Space Model	22
3.2 Wind Farm + OLTC Voltage Control	24

3.2.1	Optimisation	25
3.2.2	State Space Model	26
3.3	Wind Farm + VSC-HVDC Voltage Control	27
3.3.1	Optimisation	28
3.3.2	State Space Model	29
3.4	Power Factory	31
3.4.1	Wind Farm Voltage Control	31
3.4.2	Wind Farm + OLTC Voltage Control	34
3.4.3	Wind Farm + VSC Voltage Control	35
3.5	Results and Discussion	36
3.5.1	Wind Farm Voltage Control	36
3.5.2	Wind Farm + OLTC Voltage Control	38
3.5.3	Wind Farm + VSC Voltage Control	41
3.5.4	Discussion	42
4	Network Coordination	45
4.1	Wind Farm + External OLTC Voltage Control	45
4.1.1	Optimisation	46
4.1.2	State Space Model	48
4.2	Power Factory	48
4.3	Results and Discussion	49
5	Conclusion	53
5.1	Future Work	54
6	Conclusiones	55
	Bibliography	57
	Appendix A	61
	Appendix B	65

List of Figures

1.1	EU Power Mix in 2000 and in 2015 [3]	1
1.2	Danish Wind Power Capacity and Share [6]	2
2.1	MPC Time Description [28]	11
2.2	MPC Controller and System Integration	11
2.3	Admittance Profile	16
2.4	Voltage Profile	16
2.5	Voltage Magnitude Sensitivity to WT10 VAR injection	17
2.6	Voltage Magnitude Sensitivity to 1-p.u. Increment in V_{POC}	18
2.7	Voltage Magnitude Sensitivity to a Tap-Down Step	18
3.1	VAR Capacity Curve of Type 4 WTG	22
3.2	AVR control of a OLTC transformer [36]	27
3.3	VSC Control Scheme	30
3.4	Nordic32 Power System [40]: Single-Line Diagram	32
3.5	Wind Farm Network: Single-Line Diagram	33
3.6	Voltage Controller Scheme	33
3.7	WTG Scheme	34
3.8	OLTC Scheme	34
3.9	Wind Farm VSC Scheme	35
3.10	Wind Farm Active Power Output	36
3.11	WFVC: Voltage Magnitude at POC and MV buses	37
3.12	WFVC: Voltage Magnitude and Reactive Power of WTGs	38
3.13	WF+OLTC VC: Voltage Magnitudes	39
3.14	WTGs: Voltage Magnitude & Reactive Power	40
3.15	WF+OLTC VC: OLTC Tap Change Detail	40
3.16	WF+VSC VC: Voltage Magnitude at POC and MV buses	41
3.17	WF+VSC VC: VSC WF-Terminal Outputs	42
3.18	VC Comparison: Voltage Magnitude at POC and MV buses	43
3.19	VC Comparison: WT7 and WT8 Voltage Magnitudes	43
4.1	External Distribution Network: Single-Line Diagram	45
4.2	Variable Load:VAR consumption	46
4.3	Voltage Control Scheme	49

4.4	Voltage Impact in Bus 1042 due to Variable Load	49
4.5	Voltage Profile within the WF	50
4.6	Voltage Profiles of Variable Load Network	50
4.7	Tap Position of $OLTC_2$	51

List of Tables

3.1	VSC Parameters	30
3.2	Voltage Controller Error Comparison	44
4.1	Voltage Profile Error Comparison	51
1	Sample of Line Admittances of the WF	61
2	Sample of Voltage Measurements at t_{70}	62
3	Voltage Magnitude Sensitivity to Q Injections	63
4	Voltage Magnitude Sensitivity to V_{POC}	64

Nomenclature

Acronyms

<i>AC</i>	Alternating Current
<i>AVR</i>	Automatic Voltage Regulator
<i>DC</i>	Direct Current
<i>DSO</i>	Distribution System Operator
<i>EU</i>	European Union
<i>FACTS</i>	Flexible AC Transmission System
<i>FRT</i>	Fault Ride Through
<i>GW</i>	Gigawatts
<i>HV</i>	High Voltage
<i>HVDC</i>	High Voltage Direct Current
<i>IEEE</i>	Institute of Electrical and Electronics Engineers
<i>LV</i>	Low Voltage
<i>LVRT</i>	Low Voltage Ride Through
<i>MPC</i>	Model Predictive Control
<i>MPPT</i>	Maximum Power-Point Tracking
<i>MSE</i>	Mean Squared Error
<i>MV</i>	Medium Voltage
<i>MW</i>	Megawatts
<i>OLTC</i>	On-Load Tap Changing
<i>PCC</i>	Point of Common Coupling

<i>PI</i>	Proportional-Integral Controller
<i>PLL</i>	Phase Locked Loop
<i>POC</i>	Point of Connection
<i>PV</i>	Photovoltaic
<i>QP</i>	Quadratic-Programming
<i>RMS</i>	Root-Mean-Square
<i>SVC</i>	Static VAR Compensator
<i>TSO</i>	Transmission System Operator
<i>VAR</i>	Volt-Ampere Reactive
<i>VSC</i>	Voltage Sourced Converter
<i>WP</i>	Wind Power
<i>WT</i>	Wind Turbine
<i>WTG</i>	Wind Turbine Generator

Symbols

Δu_{int}^d	Internal Control Voltage Magnitude Increment
Δi_{PI}^d	PI-controller Current Increment
Δn_{tap}	Tap Step Increment
Δn_{tap}^{ref}	Tap Step Reference Increment
ΔQ	Reactive Power Increment
ΔQ^{ref}	Reactive Power Reference Increment
ΔT_d	Discretisation Period
ΔT_p	Prediction Period
Δu_s^{d-ref}	Voltage Magnitude Reference Increment
Δu_s^d	Voltage Magnitude Measurement Increment
ΔV	Voltage Increment
ΔV^{pre}	Predicted Voltage Error
\mathcal{N}	Set of Buses in the network

S	Set of Slack Buses in the network
Re	Real Part of a Number
θ	Phase
C_f	Filter Capacitance
I	Current
k_{o_i}	VSC Outer-loop Integral Gain
k_{o_p}	VSC Outer-loop Proportional Gain
N_B	Number of Buses in the network
N_c	Number of Control Steps
N_p	Number of Prediction Steps
N_s	Number of Predictions in each Control Step
N_W	Number of WTG Buses in the network
P	Active Power
P^{av}	Available Wind Power
P^{ext}	External Active Power from WTG
P_m^d	VSC d-axis Modulation Index
P_m^q	VSC q-axis Modulation Index
Q	Reactive Power
R	Resistance
S	Apparent Power
T_c	Control Period
T_d	VSC Time-constant Delay
T_p	Prediction Horizon
T_{inr}	VSC Inner-loop Time-constant Delay
u^d	d-axis Voltage
u^q	q-axis Voltage
V	Voltage

V^{ref}	Voltage Reference
V^{th}	Voltage Threshold
X	Reactance
Y	Admittance
Y_{bus}	Admittance Matrix
Z	Impedance

CHAPTER 1

Introduction

1.1 EU Future Objectives

Once climate change was recognised as a fact through the Kyoto Protocol, the European Union (EU) set several energy strategies for next decades in order to tackle it. Some targets must be achieved by 2020 and 2030 in order to reduce greenhouse gases. Among them, it is highlighted a 20% of minimum renewable energy contribution in the total electricity consumption by 2020 [1]. Thus, promoting the investment in new sustainable sources of energy production instead of conventional fossil fuel power.

Some other governments, such as the Danish, went a step further on their climate policies. In this case, aiming at a 30% of renewable production to supply its total energy consumption for the same date as before stated [2].

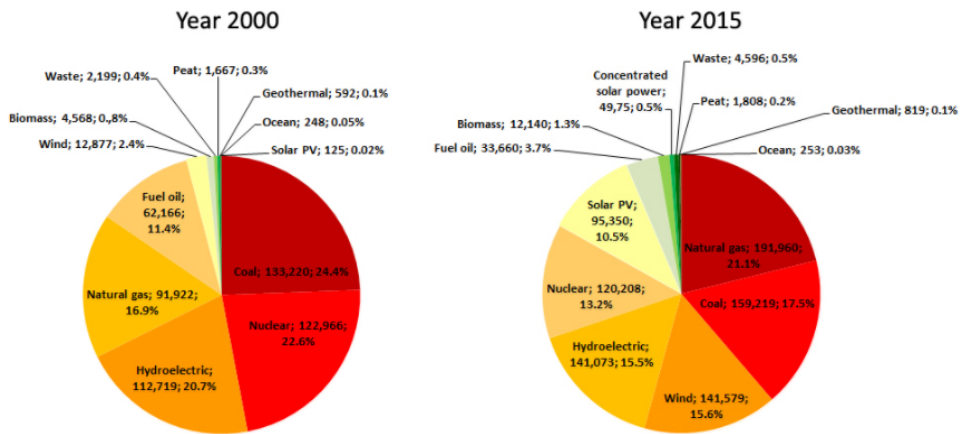


Figure 1.1: EU Power Mix in 2000 and in 2015 [3]

This framework pushed up the growth of renewable sources' share as it can be seen in Figure 1.1. The total power capacity was increased from a 24% to a 44%.

A promising jump backed up by the policies mentioned before, even they were only committed from 2008 on.

Moreover, a deeper analysis of renewable sources can be done. This suggests a huge development of wind energy. Firstly, it stands as the power source which more has increased its capacity, with almost 130 GW installed along that period. Even more than the natural gas. Secondly, it beats hydro power and gets its historic first position as the main renewable energy source. Later on, figures from 2016 provides even further success. While an 86% of new power installations are of renewable sources, more than the half of them are related to wind energy. In addition, wind power defeated coal in the capacity power mix [4]. It means that wind power represents the second largest source of energy of the whole EU.

A particular good example of wind energy development, and so renewable energy, is Denmark. In this case, wind power production overtook a 40% of domestic power supply in 2015 [5] against a 10% in the EU. Furthermore, the Danish effort also represents a new trend in installed capacity related to offshore wind power. These previously mentioned figures can be seen in the following Figure 1.2.

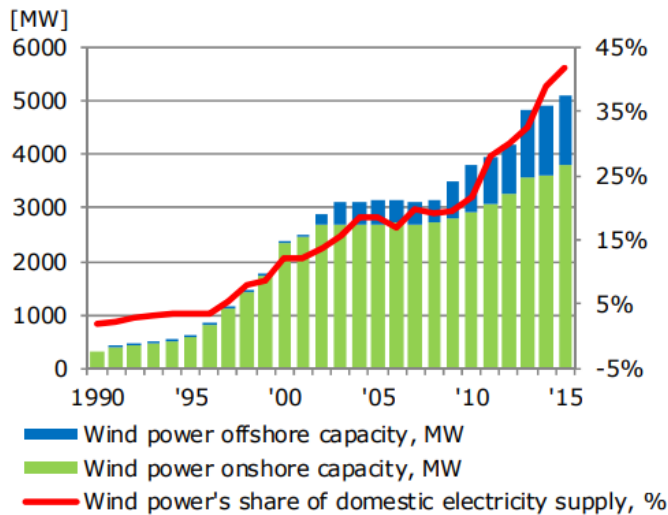


Figure 1.2: Danish Wind Power Capacity and Share [6]

New projects regarding wind power far from land (offshore) might push forward the renewable growth. They have the same advantages as onshore wind power. Moreover, faster and more constant wind speeds make the same turbines produce more

energy. For this reason, bigger wind turbines and larger wind farms are topics of interest. Among those, it can be found wind farms of the same capacity of conventional power plants. Thus, satisfying both reduction of greenhouse gas emission and raising the share of sources of green energy. What helps speeding up the decarbonisation process established at the EU objectives.

1.2 New Power System Challenges

As it has been shown in the previous section, the renewables have been pushed forward due to environmental policies and a sustainable attitude. However, it is not all about good actions installing renewables all around. It challenges the power system, the actual structure which is holding up the changes regarding electric energy generation.

Historically the power system has been a network connecting generators of electricity to customers through transmission and distribution grids. A model which was defined as centralised. Based on large power plants settle down close to their source of energy such as coal mines or harbours importing oil and gas. They were sending energy far away to the points of consumption. Moreover, the flow of energy was strict to only one-direction: generation – transmission – consumption.

The first challenge comes up with utility-level renewable sources such as wind farms and photovoltaic (PV) solar farms since they can be installed closer to the points of consumption. What means that power losses are lower even if they are not sent at really high voltages. Thus, large step-up transformers and high voltage lines are not needed for this new configuration.

Second, a new agent is defined as ‘prosumer’ who threatens the one-direction established rule. This customer of energy is connected to the distribution grid, as usual. However, this new agent has a new function which is generating energy with for example PV panels. Depending on their consumption and generation, they can be either a traditional sink or otherwise, a source of electricity. A fact which causes modifications on power flow directions and voltage profiles of the network.

The third and more critical issue regards power system operation. For so long time, conventional generators were set to follow a constant power reference according to the energy demand at that moment. Consumption patterns are predictable and they are calculated with certain accuracy. However, renewable sources can not follow a set-point all the time. The most important drawbacks are their uncertainty and variability. The former one makes it extremely difficult to forecast their instantaneous maximum production, so their power share to the system. The latter makes trouble on real-time operation. Continuous variations on weather conditions make fast and

large changes on energy injections. For these reasons, fast conventional generators are still needed as backup of the system to meet production and consumption levels.

These issues are only some of the actual concerns of the electricity system and all their agents involved in. In spite of these challenges, the network must provide electricity of quality to the points of consumption. For this reason, the grid codes were created. They set the requirements of the power supply in order to ensure a good quality energy service.

1.3 Grid Codes

Grid codes can be defined as a framework of technical regulations which ensures a secure power system performance in order to supply good quality energy to the consumption points. Each Transmission System Operator (TSO) rules all the agents connected within the same network, from generators to customers.

As system performance depends on many agents and their electric parameters at the point of connection, a series of secondary services are classified as ancillary services according to each technical parameter addressed [7]: scheduled power generation, frequency/active power control, voltage/reactive power control, inertial response, fault ride through, fault current contribution, etc.

Among these regulations, frequency and voltage might be the most important parameters to take into account. The former one characterises the whole system frequency and represents all the synchronous elements working in a specific area. The latter one states the set-point at each system level in order to provide a good quality service to each consumer. For that reason, they were the minimum requirements at the point of connection (POC) that a renewable energy producer had to satisfy some years ago.

However, the regulations and minimum requirements are changing along the time due to a challenging increment of share of renewables. As more conventional power plants are closed, there are less agents providing ancillary services for a secure system. Moreover, there are more variations on generation and so, more risk of system disturbances. Therefore, more services and more strict requirements are now asked to renewable energy producers.

1.4 Master Thesis' Objective

First of all, this project is an extension of the research study carried out in [8].

As it is stated previously, offshore wind farms are a current spotlight because of its potential. They can supply larger amounts of power to the grid in order to further increase the share of renewables even substituting conventional power plant of large size. However, they represent a big challenge for the energy sector. First, larger amounts of power mean higher voltage variability and stability issues within the wind farm. Second, these effects are transmitted into the system. So the whole system might reflect the voltage fluctuations.

For those reasons, this work aims at improving the performance of wind farms to tackle those challenges while pushing forward wind power development. Specifically, the main target of this work is the voltage control of all the buses related to the wind farm. Firstly, designing a voltage control to keep all the buses in the wind farm within limits, so that all the wind turbine generators (WTG) are working in a safe state. Secondly, analysing and coordinating new technologies to enhance the performance of the whole wind farm at the POC. Thirdly, coordinating the voltage control of the wind park with other main network devices to improve the behaviour of the main network while keeping an optimal state of the wind farm.

CHAPTER 2

Voltage Control

2.1 Theoretical Principle

A constant voltage is desired across all the nodes of a power system in order to provide a good quality electricity service to final customers. Moreover, that would mean all electrical machines and auxiliary devices are within their safety limits and close to their respective rated value. Thus, everything would be working safely and ensuring optimal operational performance. However, this ideal state is difficult to achieve due to the massive amount of interconnected devices in a network and their different dynamics. For this reason, controlling the voltage is a major concern in power system operation. Even more, with the new challenges already introduced before.

Nonetheless, ensuring the right voltage level in a grid means a deep understanding of electrical parameters. First of all, the variables which determine that level must be found. Later on, controlling their influence will be the second objective. Therefore, an analysis of the voltage parameter is developed in the following equations. An approach to the basics is carried out with a simple example [9]. In this case, the power transfer $S = P + j \cdot Q$ between two points A and B in a single line circuit is analysed through an impedance $Z = R + j \cdot X$.

$$S_B = V_B \cdot I^* = P + j \cdot Q \quad (2.1)$$

$$V_A = V_B + (R + j \cdot X) \cdot I = V_B + (R + j \cdot X) \cdot \left(\frac{P - j \cdot Q}{V_B^*} \right) \quad (2.2)$$

$$\Delta V = V_A - V_B \approx \Delta V_{real} = \frac{R \cdot P + X \cdot Q}{V_B} \quad (2.3)$$

Based on Equation (2.1) and its the complex power S from the receiving B point of view, Equation (2.2) develops the voltage at the source A end. Taking into account an assumption for distribution circuits, the phase δ of the voltage is small and can be approximated to zero. Then, $V_B = V_B^* = |V_B|$. Eventually, including this assumption into Equation (2.2) allows developing the equation and split it into real and imaginary parts. Being the latter part approximate to zero because of the distribution circuit assumption again. Finally, the voltage increment ΔV between two nodes is presented

in Equation (2.3).

Next, the variables which influence the voltage can be analysed. According to (2.3), the voltage at a bus depends on two aspects. First, its reference level or directly linked bus due to the connection itself. Second, a couple of variables which depends on the power transfer and hence, on the active P and reactive power Q demanded on a load at the receiving terminal. Active power is not considered in this analysis since it is assumed as fixed due to two reasons. Firstly, in the case of a load its operation depends directly on P , then a right behaviour is not pretended to be compromised. Secondly, in the case of a source such as a wind farm its revenue depends on the active power injected and hence, it is maximised to actual weather conditions and non-control is expected. Consequently, reactive power takes over the responsibility as the variable for voltage variation.

For this reason, reactive power stands out for being in charge of the primary voltage control as suggested in [10]. It is considered as a local problem of an area and hence, a reactive power balance must be kept across the devices within this area. These devices can be gathered in two groups: sources or sinks of Q . The former group joints the following devices: overexcited synchronous generators, shunt capacitors banks, capacitances of overhead lines and cables and, Flexible AC Transmission Systems (FACTS). On the other hand, the sinks are the following: underexcited synchronous generators, inductive motors and loads, shunt reactors, inductances of overhead lines, cables and transformers and, FACTS. Furthermore, the last wind turbine models such as type 3 and type 4 also provides reactive power support with their converter technology. Reactive power capability which can work in any of the groups presented. It is justified by a series of control modes or controller diagrams suggested in [11] in order to emulate the automatic voltage regulator (AVR) of conventional synchronous generators.

2.2 Literature review

Voltage control has been studied for a long time and hence, a wide range of topics are covered in its state-of-the-art. Although decentralised or machine level controllers were of interest, this research study is focused on wind farm voltage control level. Within this area, a long classification of techniques is described as follows. First, voltage analysis can be subdivided into controllers and optimisation. Second, the time-horizon of different methods is suggested. Third, a series of objectives are covered. Fourth, voltage or VAR support is sorted by controlled devices.

First of all, voltage controllers for park level are usually a PI emulating the AVR of a traditional machine as suggested in [12, 13]. They can integrate features like drop compensation or feedback loops as presented in the former source. Otherwise, the latter one proposes a coordination of different hierarchical levels of controllers

for faster actions. While all these controllers are implemented for fixed real-time purposes, [14] introduces a series of controllers which are shifted depending on the state of grid parameters. Thus, proposing a series of control strategies joint under the term VAR optimisation method. Later on, more advanced designs have evolved into optimisation algorithms gathering different time-scales, objectives and devices.

Secondly, the time-horizon is a control parameter to take into consideration. In [15, 16], VAR control strategies are dependent on the time frame. From milliseconds to seconds, the objectives are low voltage or fault ride through (LVRT or FRT). From seconds to minutes, it addresses voltage stability, power factor or flicker mitigation. Then, for longer periods the strategies are VAR support to the system or power loss minimisation. On the other hand, time-dependent parameters such as wind speed or consumption load are considered in the study of [17]. It analyses the benefits of introducing forecast data of those variables in the optimisation. However, the results show that if a perfect knowledge of the variables is not available, the performance is similar to a simple voltage controller. Hence, [18] takes a different approach. It suggests an hourly optimisation which provides the reference for the wind power plant controller for that time. An extreme application of this long-time voltage control calculation is studied in [19] for planning purposes. Therein, the allocation of VAR-support devices is assessed.

Thirdly, an optimisation algorithm can be in charge of different objectives. While the voltage control is considered the main one for this project, secondary targets might bring some benefits for the wind farm. From the more basic power factor control in [14], then a maximum power-point tracking (MPPT) in [20] and even the economically evaluation from [19, 21]. On the other hand, a more often goal is the power loss reduction which is reviewed in [18, 20, 22, 23].

Fourthly, the device taking over the VAR support is another factor. Based on the VAR contribution of WTGs, auxiliary electrical machines are integrated in the voltage control. The reactive power supply is enhanced by a static VAR compensator (SVC) in [16, 20, 22]. Network topology is modified by an OLTC transformer in [17, 22]. Furthermore, a decoupled network connected through HVDC is applied in [24, 25]. In this case, the voltage control is carried out by their converter which handles the voltage of the DC-link. Then, introducing a coordination among the devices connected to that multiterminal DC grid.

Further coordination is explained in [26]. It develops an optimisation algorithm with some of the previous methodologies explained above. That is a voltage control based on an incremental linear problem adjusting VAR responses to minimise power losses. Also, coordinated responses from WTGs, an OLTC and an SVC. Furthermore, it introduces a technique based on sensitivity coefficients for integrating power system influences. Thus, being this example an approach to the MPC method explained below and carried out along the project.

2.3 Model Predictive Control

Model predictive control (MPC) is an advanced control technique which has been used for long time in manufacturing and processing industries [27]. More recently, it has been extended to power systems and other subsystem networks [28]. Its main feature is gathering three principles: modelling, prediction and optimisation. Firstly, an approximate linear model represents the dynamics of every element of the system at the same time that it integrates influences among the subsystems. Secondly, the control problem includes a fixed interval of time and it is solved along the time-horizon. For this reason, this method takes into account the behaviour and long-term effect of the model over the finite-horizon. Thirdly, the control actions are decided according to an optimisation problem. Thus, an optimal solution is found for each time step, although only the first control action is applied and kept along that control period [29].

It is suitable for power system control because of the following advantages. First, its dynamic model captures both fast and slow responses of the systems. Thus, a coordination between devices is feasible. For instance, the relatively fast response of WTG converters can be integrated to slow tap changes of transformers, taking into consideration the long-term effects of each one. This system modelling lays on the state space model from Equation (2.4). Second, the optimisation problem allows flexibility. In this project, a voltage control strategy has been pointed out. It joins different voltage targets across the network. However, a multi-objective function could also have been implemented in order to reduce system losses or operational cost. Third, this kind of problem again stands out due to its ability to handle constraints. A key aspect to capture real performance of the machines taking into account either their operational limits or grid operational requirements. An optimisation problem can be seen in (2.5), where both objective function and constraints are described.

$$\begin{aligned} \dot{x} &= A \cdot x + B \cdot u \\ y &= C \cdot x \end{aligned} \tag{2.4}$$

$$\begin{aligned} \min \quad & \sum_{k=1}^{N_p} (\varepsilon^2(V)) \\ \text{Subject to :} \quad & V_{min} < V < V_{max} \end{aligned} \tag{2.5}$$

Once the working principle and advantages of the MPC have been presented, the time-domain variables must be clarified for deeper understanding. These variables are: the prediction horizon T_p , the control period T_c and the prediction period ΔT_p . They are sorted from bigger to smaller time duration. Their selection must be careful since the accuracy of the whole control depends on them. Therefore, the prediction horizon must gather all the long-term effects of the subsystem and the prediction steps must follow the fast dynamics of the machines. Instead of time duration, they also can be identified as number of steps along the prediction horizon as follows: the

number of predictions in each control step is $N_s = \frac{T_c}{\Delta T_p}$, there are the following control steps $N_c = \frac{T_p}{T_c}$, then the total number of prediction steps is $N_p = \frac{T_p}{\Delta T_p}$. The time-domain variables meaning can be found in Figure 2.1 as a example.

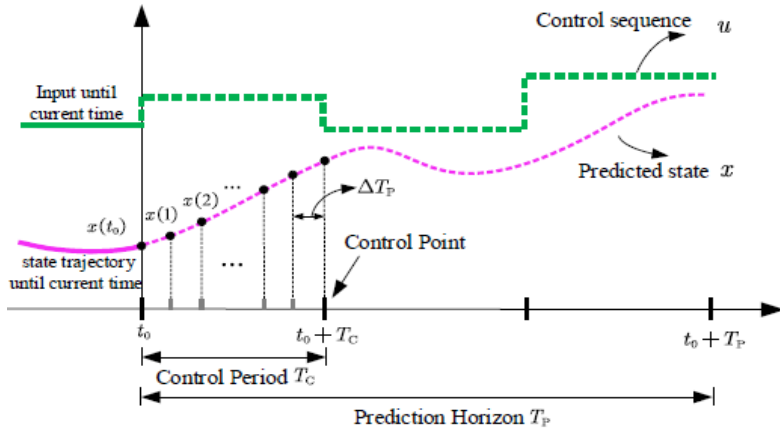


Figure 2.1: MPC Time Description [28]

Regarding the MPC application, a methodology for integration is illustrated in Figure 2.2. On the left side, an MPC algorithm is implemented in a software such as Matlab while reading both references and measurements of actual operation of the system. On the right side, the power system with its devices (machines, controllers and sensors) are implemented. Finally, a communication is needed between both sides for a feedback control implementation. Along the project both parts, algorithm and system model are explained more in detail.

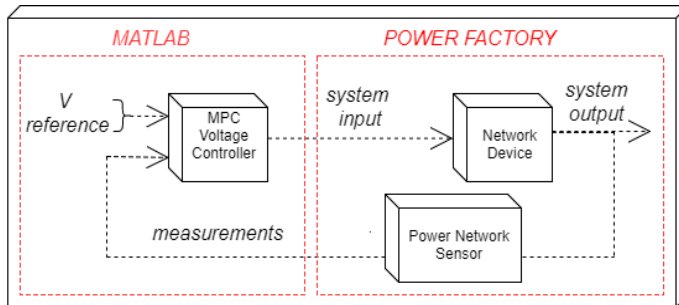


Figure 2.2: MPC Controller and System Integration

2.4 Sensitivity Coefficients

Sensitivity coefficients are used in power system control to relate control variables to controlled parameters based on linear-model approaches. It helps an algorithm such as the MPC to aggregate the current and/or predicted effects of control variables with their affected grid parameters. As it is suggested in [30], the traditional method consists of updating the Jacobian matrix of the load flow analysis. However, this approach has two drawbacks. First, the computational burden and processing time. This method updates the Jacobian for each iteration according to the current state of the network. What means building and inverting a matrix of the size of the network. Second, this technique does not provide a unique solution for each iteration. Furthermore, neither Newton Raphson nor fast decoupled load flow methods find a convergent solution for this problem as it is explained in [31]. For these reasons, the Jacobian approach does not seem convenient for real-time applications and the first source proposes a new methodology.

It must be highlighted that the scope of those research studies is radial distribution networks. This kind of grid is characterised by its high R/X ratio. In spite of that fact, a similar structure is found on the radial structure and long MV feeders (high R/X ratio) of traditional wind farms. Thus, those study results are considered of interest and hence, their proposals are implemented in this project. Further on, it is justified by the use of this calculation method in similar wind farm research studies such as [8], [28] and [32].

Eventually, the application of this computational efficient method, and specifically in the wind farm case, is based on a series of assumptions. Considerations needed for backing up the mathematical development shown below and its unique solutions. Thus, they must be emphasised even though some have been already commented.

- Slack bus voltage magnitude and angle remain constant independently of the power injections
- PQ injections are considered constant and independent of bus voltages
- While there is a PQ injection change in a bus, all the other power injections remain constant
- The partial derivatives showed have a unique solution for every radial distribution network
- The wind farm network is considered as radial distribution network due to its topology

2.4.1 Sensitivity to Q Injections

As one of the main targets of this project is a coordinated wind farm voltage control, the sensitivity coefficient of interest is related to the voltage magnitude. As WTGs are one of the technologies controlling the voltage, their reactive power effect over the voltage magnitude must be demonstrated. The efficient analytical computational method demonstrated by [30] is explained in the following lines starting with the relationship between complex power S and complex voltage V .

$$\bar{S}_i = \bar{V}_i \cdot \sum_{j \in \mathcal{N}} (Y_{bus}(i, j) \cdot V_j) \quad (2.6)$$

Where \bar{S}_i and \bar{V}_i are the conjugates of their respective complex numbers, Y_{bus} is the admittance matrix of the network and, i and j are bus identifiers which belong to the set $\mathcal{N} = \{1, 2, \dots, N_B\}$. Where N_B represents all the buses of the wind farm.

Next, the derivation of the voltage in regards to the VAR injection in a bus $l \in \mathcal{N}$ is carried out in Equation (2.7). This suggested calculation provides a linear equation to the unknown voltage derivative variables. Moreover, it has a unique solution for the radial distribution network assumption. This solution is equal to '-j1' when $i = l$ and, '0' for the rest of cases.

$$\frac{\partial \bar{S}_i}{\partial Q_l} = \frac{\partial \{P_i - jQ_i\}}{\partial Q_l} = \frac{\partial \bar{V}_i}{\partial Q_l} \cdot \sum_{j \in \mathcal{N}} (Y_{bus}(i, j) \cdot V_j) + \bar{V}_i \cdot \sum_{j \in \mathcal{N}} \left(Y_{bus}(i, j) \cdot \frac{\partial V_j}{\partial Q_l} \right) \quad (2.7)$$

Later on, a system of equations is set individually with the real and imaginary part of the previous equation and its solutions. Besides, two principles are needed for their development. First, the derivative of the conjugate of a complex number is equal to the conjugate of the derivative of that complex number. Second, the equations of *Cauchy–Riemann* are implemented. This procedure provides the value of the partial derivatives associated with voltage sensitivity. Finally, the desired voltage magnitude sensitivity to VAR injection is calculated with the following equation.

$$\frac{\partial |V_i|}{\partial Q_l} = \frac{1}{|V_i|} \cdot \text{Re} \left(\bar{V}_i \cdot \frac{\partial V_i}{\partial Q_l} \right) \quad (2.8)$$

2.4.2 Sensitivity to Slack Bus

As voltage magnitude is the main goal of the analysis, it must be related to different parameters. Once the reactive power has been explained as a voltage influence agent, the voltage change of a reference bus is indeed another one. It must be, of course, a strong or reference bus to make a considerable modification. For this reason, the second agent of influence is the voltage magnitude change in an assumed slack bus. The analysis starts again in Equation (2.9) with the relationship between the

conjugates of complex power \bar{S}_i and complex voltage \bar{V}_i . Now, \mathcal{S} is the set of slack buses which respects this assumption: $\mathcal{S} \cup \mathcal{N} = \{1, 2, \dots, N_B\}$ and $\mathcal{S} \cap \mathcal{N} = \emptyset$.

$$\bar{S}_i = \bar{V}_i \cdot \sum_{j \in \mathcal{S} \cup \mathcal{N}} (Y_{bus}(i, j) \cdot V_j) \quad (2.9)$$

Then, the partial derivative with respect to the voltage magnitude of the slack bus is developed as shown in Equation (2.10). This voltage magnitude belongs to: $V_k = |V_k| \cdot e^{j\theta_k}$, where the reference or slack bus $k \in \mathcal{S}$ and the solution of the derivation is: $\frac{\partial \bar{S}_i}{\partial |V_k|} = 0$.

$$\frac{\partial \bar{S}_i}{\partial |V_k|} = \frac{\partial \bar{V}_i}{\partial |V_k|} \cdot \sum_{j \in \mathcal{S} \cup \mathcal{N}} (Y_{bus}(i, j) \cdot V_j) + \bar{V}_i \cdot \sum_{j \in \mathcal{S} \cup \mathcal{N}} \left(Y_{bus}(i, j) \cdot \frac{\partial V_j}{\partial |V_k|} \right) \quad (2.10)$$

Taking into account the following specific term for the slack bus:

$$\frac{\partial}{\partial |V_k|} \sum_{j \in \mathcal{S}} (Y_{bus}(i, j) \cdot V_k) = Y_{bus}(i, k) \cdot e^{j\theta_k} \quad (2.11)$$

previous Equation (2.10) and its solution can be formulated as:

$$-\bar{V}_i \cdot Y_{bus}(i, k) \cdot e^{j\theta_k} = \frac{\partial \bar{V}_i}{\partial |V_k|} \cdot \sum_{j \in \mathcal{S} \cup \mathcal{N}} (Y_{bus}(i, j)) \cdot V_j + \bar{V}_i \cdot \sum_{j \in \mathcal{N}} \left(Y_{bus}(i, j) \cdot \frac{\partial V_j}{\partial |V_k|} \right) \quad (2.12)$$

Eventually, this equation is linear in regards to voltage partial derivatives according to the methodology suggested in [30]. Partial derivatives which are the unknowns of a system of equations with a unique solution for the assumed radial distribution network or wind farm in this case. Therefore, the sensitivity solution is the following Equation (2.13). But the target of this section is voltage magnitude sensitivity to voltage magnitude change of the slack bus, so only the real part is of interest later on and it is shown in Equation (2.14).

$$\frac{\partial V_i}{\partial |V_k|} = \left(\frac{1}{|V_k|} \cdot \frac{\partial |V_i|}{\partial |V_k|} + j \cdot \frac{\partial \theta_i}{\partial |V_k|} \right) \cdot V_i, \quad \forall i \in \mathcal{N} \quad (2.13)$$

$$\frac{\partial |V_i|}{\partial |V_k|} = |V_i| \cdot \operatorname{Re} \left(\frac{1}{V_i} \cdot \frac{\partial V_i}{\partial |V_k|} \right) \quad (2.14)$$

2.4.3 Sensitivity to Tap Changes

An OLTC is considered also an agent of influence on the voltage. It makes a direct effect into the voltage magnitude, which is the main target of the sensitivity

analysis carried out along this section. This effect is related to a tap position increment Δn_{tap} . For this reason, the voltage magnitude change due to a tap step must be quantified with the following explanation.

Each tap transformer change is strongly related to the voltage magnitude change in the slack bus presented in previous section. Therefore, all the previous equation development is useful as well in this coefficient analysis. Taking into account that the HV-side terminal of the OLTC is now the assumed slack bus k . Then, Equation (2.15) introduces the sensitivity to a tap position change.

$$\frac{\Delta|V_i|}{\Delta n_{tap}} = \frac{\partial|V_i|}{\partial|V_k|} \cdot \Delta V_{tap} \quad (2.15)$$

Where the first term of partial derivatives corresponds to the results from Equation (2.14). In addition, ΔV_{tap} is the voltage magnitude step related to each tap step. What is considered as a main feature set by the transformer manufacturer and in this case is equal to 1.25% of the rated voltage in each terminal.

Eventually, a couple of considerations regarding the tap change sensitivity. Firstly, it is considered as a discrete magnitude due to its discrete tap positions. Secondly, the voltage magnitude step effect is expected to happen only in the LV-terminal of the OLTC due to the electrical coupling of the HV-side with the main network.

2.4.4 Sensitivity Analysis Results

The sensitivity coefficients calculated depend directly on two aspects. First, the network topology which is kept constant in a simulation. Second, the current state of the system measured through the bus voltages. Since the latter one is changing all the time, a random calculation is chosen as an example. Thus, the results shown below corresponds to the system state at 70 seconds of a simulation which is explained later. In Figures 2.3 and 2.4 both parameters, topology and voltages are illustrated. In this case, one of the four feeders (from WT8 to WT10) of a wind farm has been chosen as an example. For further detail about the Y_{bus} or the voltage measurements of this example, they are in Tables 1 and 2 in Appendix A.

First of all, the sensitivity to reactive power injections is calculated following the guidelines presented above. The system of equations resolution is shown in Appendix B through a script. Solving this system of equations developed from Equation (2.7), the sensitivity of complex voltage to Q injections is found. Then, this solution is introduced in Equation (2.8). Thus, the results of this equation are the expected sensitivity of voltage magnitude to Q injections. The complete set of results for each bus is shown in Table 3 in Appendix A. However, a brief visual results can be observed in Figure 2.5. There, the voltage magnitude changes according to $1MVAr$ of change in WT10. In the upper part, the feeder of this wind turbine is represented together

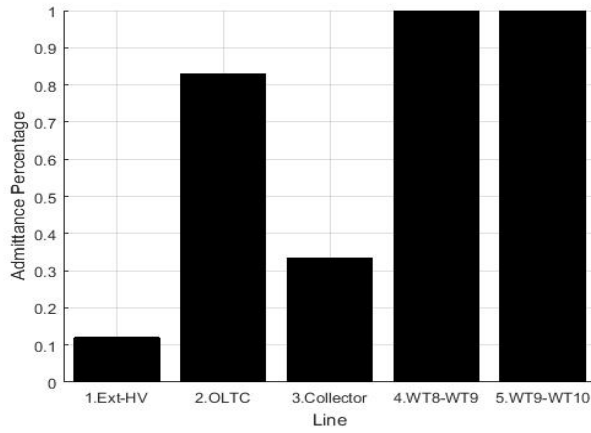


Figure 2.3: Admittance Profile

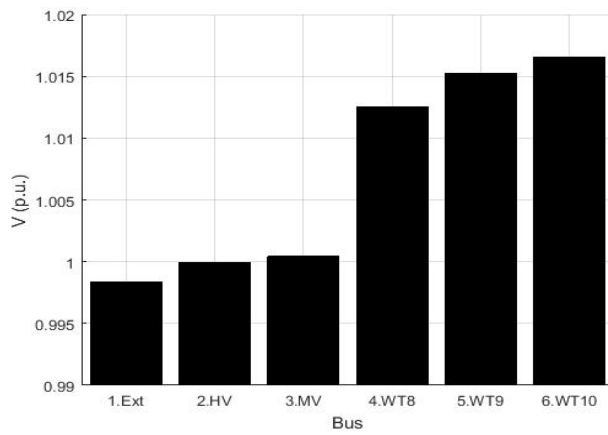


Figure 2.4: Voltage Profile

with the main buses of the WF. Below, another feeder of WTGs is shown to give an example of how a single WTG influences all the other voltages.

Secondly, the voltage magnitude sensitivity to voltage magnitude change of the reference bus is calculated. Following the same procedure, a system of equation is set from Equation (2.12). This is also explained through the Matlab code in Appendix B. The solution of this system provides the derivative term needed in Equation (2.14). Next, the desired coefficients are found. These coefficients represent the rate of change of voltage magnitude in each bus according to the voltage magnitude change in the reference bus (POC). Method used for instance for a HVDC-converter control. Some adjustment is needed for a good comprehension of these parameters. In this case *Adjustment 1* calculates these coefficients divided by the ratio given for the POC bus. Then, getting the rate of change in each bus for a unity change in the reference. A sample of the results are illustrated in Figure 2.6 for the main MV collector bus and for the WTGs of the second feeder of the WF. Further detail with all the coefficients is stated in Appendix A.

Thirdly, the sensitivity to OLTC tap changes is worked out. In this case, the coefficients are related to the previously calculation since they are also due to voltage changes. For this reason, the same procedure is carried out in order to find the parameters. However, a different adjustment is needed this time. Assuming a strong coupling of the POC bus to the external network, non reaction is going to be found in the HV-side of the OLTC. Therefore, this value must be set to zero and its ratio must be added to the rest of nodes with the opposite direction effect. The results of the adjustment (*Adjustment 2*) are gathered in Appendix A with the previous ones. Nonetheless, the direct coefficients of a tap change are found multiplying those voltage-

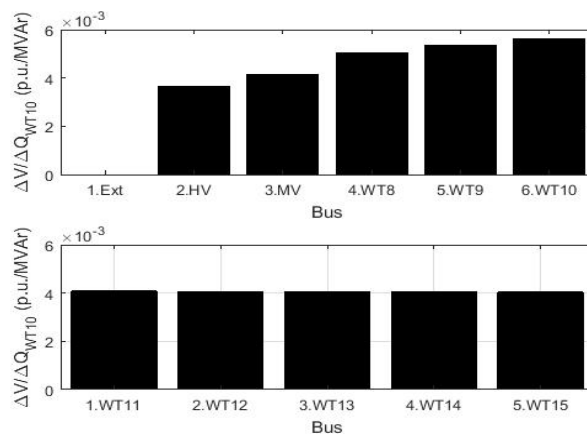


Figure 2.5: Voltage Magnitude Sensitivity to WT10 VAR injection

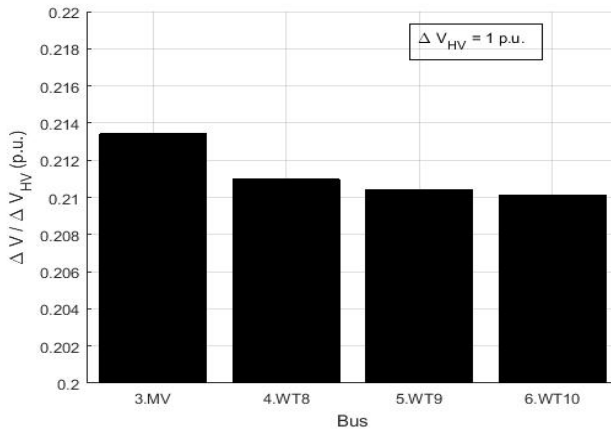


Figure 2.6: Voltage Magnitude Sensitivity to 1-p.u. Increment in V_{POC}

change values by the voltage increment of each tap step, according to Equation (2.15). A sample of these coefficients at some of the buses are illustrated in Figure 2.7.

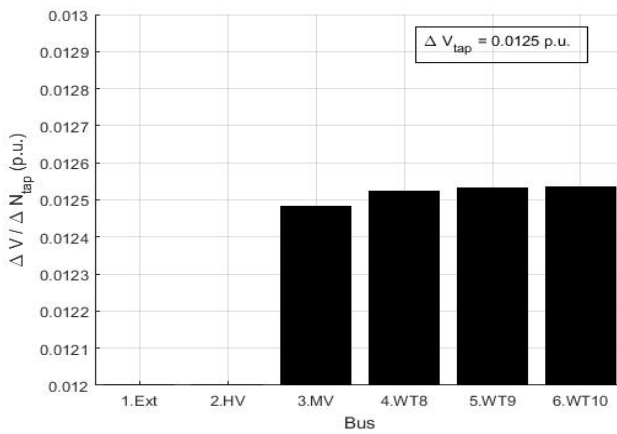


Figure 2.7: Voltage Magnitude Sensitivity to a Tap-Down Step

CHAPTER 3

Wind Farm Coordination

Once a MPC has been chosen as a voltage control technique, the reactive power capability of WTGs is going to be presented as the first strategy. After, a coordination with other devices is explained in this chapter, aiming at better behaviour of bus voltages profile. In the previous research work, a wind farm was coordinated with an automatic OLTC transformer and a static var compensator (SVC). Now and as a second strategy a controllable tap transformer is analysed to dismiss the need of fast and expensive VAR devices such as the SVC. Besides, the increasing attention in high voltage direct current (HVDC) cables makes it a topic of interest for integrating them into the voltage control framework as the third strategy. Eventually, it must be clarified that the MPC voltage control is implemented as a function in Matlab. On the other hand, the network topology and physical controllers are implemented in DIGSILENT Power Factory, while a communication between the two softwares is needed.

3.1 Wind Farm Voltage Control

3.1.1 Optimisation

As it is stated in Section 2.3, the optimisation is one of the parts of the MPC. At this stage, a decision-making process is carried out in order to decide the control actions needed for the following prediction horizon. Even though, only the first control action is applied. The main components of this methodology are the measured variables, the decision variables, the objective function and the constraints.

First, the measured or controlled variables. They are the network parameters to care about, so the deviation concerning their reference need to be minimised. At the same time, they are working as a flag. The MPC works in two control modes and these network measurements determine which mode is active at each iteration. The voltage measurements are the following:

- V_{POC} : Voltage at POC or high-voltage side of the OLTC
- V_{MV} : Voltage at Medium Voltage bus or low-voltage side of the OLTC
- V_{WT} : Array of voltage at wind turbine terminals

Regarding the voltage control modes, the first mode or *CorrectiveMode* takes care of all the controlled parameters. For this reason, if any of them overcomes its threshold, this mode is activated. In this way, every time there is a violation of any of the controlled variables the MPC tries to improve the voltage profile of the whole wind farm. At the same time it avoids wind turbine tripping. Then, its objective function explained below takes action. The second mode or *PreventiveMode* however, only takes care of the voltage at the POC. In this way, there is a further improvement of the main parameter of the wind farm to its common reference, since the requirements from the system operator aim at this bus. That means prevention at the main bus while all the others are working within safe voltage ranges.

Usually, the voltage magnitude reference of all the buses are considered as $V_i^{ref} = 1p.u.$. Regarding their thresholds, they are individual to keep individual targets or safety ranges. First, at the POC the threshold is $V_{POC}^{th} = 0.01p.u.$ due to its importance to system requirements. However, it depends on the grid code and system operator instructions. Second, $V_{MV}^{th} = 0.03p.u.$ due to more relaxed conditions within the wind farm. Third, $V_{WT}^{th} = 0.08p.u.$ since wind turbine protections are usually in the range of $[0.9, 1.1]$. In this way, there is still a security gap before tripping out the machine.

Second, the decision variables are the solution of the optimisation. They provide the input for the devices controlled. Specifically, in this first strategy the decision variable is: ΔQ_{WT} , an array of the reactive power supply increment of each wind turbine generator.

Third, there is a objective function (*ObjFun*: (3.1)). It consists of a minimisation since the voltage deviation from the voltage reference wants to be reduced. In this case, a quadratic error function along the whole prediction horizon has been chosen for two reasons. Firstly, it minimises the error penalising much more big deviations from the set-point. Secondly, it takes into account the future states of the devices. For this reason, it tries to minimise the error along the long term, i.e. avoiding oscillations due to different dynamic responses from different devices. For this first strategy, the prediction horizon T_p is considered as 5 seconds to capture fast dynamics of WTGs for a while. The control period T_c is 1 second and the prediction period ΔT_p is 0.5 seconds.

$$\min_{\Delta Q_{WT}} \sum_{k=1}^{N_p} (\|\Delta V_{POC}^{pre}(k)\|^2 + \|\Delta V_{MV}^{pre}(k)\|^2 + \|\Delta V_{WT}^{pre}(k)\|^2) \quad (3.1)$$

This objective function belongs to the *CorrectiveMode*. On the other hand, the *PreventiveMode* only has the first term of the equation regarding the predicted voltage error at the POC. Another feature of the equation is that it can be weighted. In that case, each term would be multiplied by different values giving less importance to the higher value during the optimisation process. For this project, all the voltages have been considered with the same importance, so the same weight is considered for each term. The development of each term of Equation (3.1) is explained here:

$$\Delta V_{POC}^{pre}(k) = V_{POC}(k) - V_{POC}^{ref} + \frac{\partial |V_{POC}|}{\partial Q_{WT}} \cdot \Delta Q_{WT}(k) \quad (3.2)$$

Where V_{POC} is the current voltage magnitude measurement before starting the MPC calculation, $\frac{\partial |V_{POC}|}{\partial Q_{WT}}$ is the sensitivity coefficient array of the voltage magnitude change at POC regarding a change of reactive power supply from each wind turbine generator and, ΔQ_{WT} states the decision variable array to be minimised.

$$\Delta V_{MV}^{pre}(k) = V_{MV}(k) - V_{MV}^{ref} + \frac{\partial |V_{MV}|}{\partial Q_{WT}} \cdot \Delta Q_{WT}(k) \quad (3.3)$$

$$\Delta V_{WT}^{pre}(k) = V_{WT}(k) - V_{WT}^{ref} + \frac{\partial |V_{WT}|}{\partial Q_{WT}} \cdot \Delta Q_{WT}(k) \quad (3.4)$$

Where each of the terms have the same meaning as in Equation (3.1) but now, they are referred to the *MV* Medium Voltage bus and the *20 WT* wind turbine nodes.

Fourth, the constraints of the optimisation problem. Capturing the operational limits of the electrical machines will provide a closer image of the actual performance of the system. For this reason, the reactive power capability of the wind turbine generators has been implemented in the model as it is shown here:

$$Q_{WT_i}^{min}(k) \leq Q_{WT_i}(k) \leq Q_{WT_i}^{max}(k) \quad (3.5)$$

$$\forall i \in [1, 20], \quad k \in [1, N_p]$$

Where Q_{WT_i} in the discrete form can be related to the decision variables as: $Q_{WT_i}(k) = \Delta Q_{WT_i}(k) + Q_{WT_i}(t_0)$. Regarding the minimum and maximum values of the reactive power of each wind turbine generator, they can be calculated as follows. The VAR capacity of each machine depends on its voltage terminal set by the network and on the active power available in the machine, which at the same time depends on the wind power available. For that reason, the VAR limits are approximated by linear interpolation of the current measurements to a look-up table which might be provided by the machine manufacturer. An example can be seen in Figure 3.1

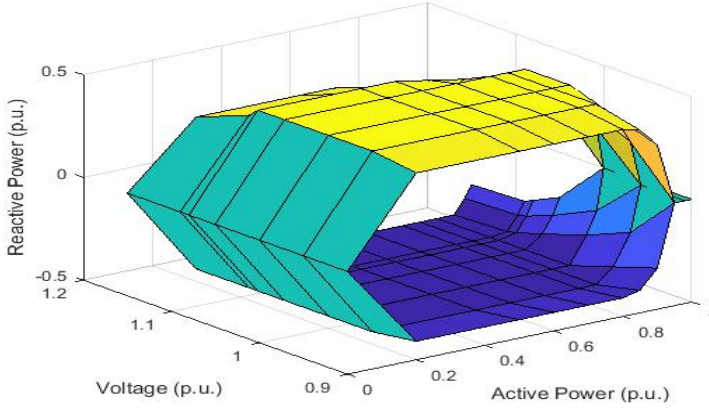


Figure 3.1: VAR Capacity Curve of Type 4 WTG

In addition, three more constraints are needed for the right behaviour of the method and the consideration of the control mode. If the MPC is working in *PreventiveMode*, the three following equations must be included as they are presented. Otherwise, in the *CorrectiveMode* they are conditional. Depending on which threshold has been violated, these conditional constraints will be considered or not. Thus, they are only included if the voltage magnitudes are within range. If they are out, the conditions must be relaxed and so, they are turn into the objective function term previously presented. The equations are the following:

$$\begin{aligned}
 -V_{POC}^{th} &\leq \Delta V_{POC}^{pre}(k) \leq V_{POC}^{th} \\
 -V_{MV}^{th} &\leq \Delta V_{MV}^{pre}(k) \leq V_{MV}^{th} \\
 -V_{WT}^{th} &\leq \Delta V_{WT}^{pre}(k) \leq V_{WT}^{th}
 \end{aligned} \tag{3.6}$$

Finally, the optimisation problem developed in this Section 3.1.1 can be formulated as a standard quadratic-programming (QP) problem. Then, it is solved with the help of two packages implemented in Matlab: Yalmip toolbox [33] and Mosek solver [34]. A fast resolution from these software allows the MPC implementation in real-time applications.

3.1.2 State Space Model

Next, it is going to be explained the modelling part of the MPC, indeed the state space model representing the dynamics of the WTGs. According to control theory, the continuous state space model of a system is represented as follows:

$$\begin{aligned}\dot{x} &= A \cdot x + B \cdot u \\ y &= C \cdot x\end{aligned}\tag{3.7}$$

Where \dot{x} is the predicted state variable, x is the current state variable, u is the input variable and y is the output variable of the model. On the other side, A , B and C are matrices associating the different variables according to the estimated behaviour of the systems.

For this simple case in which the MPC is only controlling the reactive power supply of each wind turbine, the model is represented as follows.

$$\begin{aligned}x &= [\Delta Q_{WT_1}, \dots, \Delta Q_{WT_{N_W}}]^T \\ u &= [\Delta Q_{WT_1}^{ref}, \dots, \Delta Q_{WT_{N_W}}^{ref}]^T \\ y &= [\Delta Q_{WT_1}, \dots, \Delta Q_{WT_{N_W}}]^T\end{aligned}$$

Here, the output variable array y can be identified as the decision variable array in Equations (3.2), (3.3) and (3.4) within the minimisation process. Thus, y is integrating the network model into the optimisation section of the MPC. Eventually, the decision variables are related to the input variables u . Therefore, the output of the optimisation will provide the increment in the reference and so, the value of the VAR reference for each wind turbine.

Once the system variables are explained, the matrices showing the system behaviour and the relationship among variables need to be introduced. For a wind turbine generator, a constant-Q control loop is considered as a first-order delay function. It is shown here:

$$\Delta Q_{WT} = \frac{1}{1 + s \cdot T_{WT}} \cdot \Delta Q_{WT}^{ref}\tag{3.8}$$

Where T_{WT} is a time constant of 5 seconds in the transfer function and s is the complex variable in Laplace domain. Moreover, this transfer function can be formulated in its continuous state space model as presented here:

$$\Delta \dot{Q}_{WT} = A_{WT} \cdot \Delta Q_{WT} + B_{WT} \cdot \Delta Q_{WT}^{ref}\tag{3.9}$$

Where the associating matrices are $A_{WT} = \frac{-1}{T_{WT}}$ and $B_{WT} = \frac{1}{T_{WT}}$. Thus, these matrices can be integrated perfectly into the state space model which represents the whole system. Then, A , B and C matrices from Equation (3.7) are implemented as follows:

$$\begin{aligned}A_{WT} &= \text{diag}(A_{WT}^1, \dots, A_{WT}^{N_W}) \\ B_{WT} &= \text{diag}(B_{WT}^1, \dots, B_{WT}^{N_W}) \\ C_{WT} &= \text{diag}(1_1, \dots, 1_{N_W})\end{aligned}$$

Furthermore, the system model must be discretised. This allows the integration of the discrete network measurements and the application of a methodology looking for discrete optimal solutions. In this way, the state space model in its discrete form is the following:

$$\begin{aligned}x(k+1) &= A_d \cdot x(k) + B_d \cdot u(k) \\y(k) &= C_d \cdot x(k)\end{aligned}\tag{3.10}$$

Where the discrete matrices for this and all the models presented along the project are calculated as follows:

$$\begin{aligned}A_d &= e^{A \cdot \Delta T_d} \\B_d &= \int_0^{\Delta T_d} e^{A \cdot \tau} d\tau \\C_d &= C\end{aligned}\tag{3.11}$$

3.2 Wind Farm + OLTC Voltage Control

On-load tap changing transformers or OLTC transformers are traditionally been used in active distribution networks [35]. This device installed in a substation deals with both load variation of the downstream grid and possible distributed generation. Since both of them are causing voltage variations and deviations from the original reference, this expensive solution is justified. A problem that is extrapolated to what happens in wind farms.

The OLTC transformer tries to follow the voltage reference adjusting the tap position of their inner connections. Positions that change the number of turns in a winding and then, modifies the transformer ratio. This means altering the voltage step from primary to secondary and so, keeping voltage output within expected limits. Usually, it consists in a slow mechanical process set in this project to 5 seconds that jumps one by one across the 17 discrete positions. This slow procedure is because of two reasons. First, none of the two main windings can be opened in order to avoid dangerous sparks. Second, neither the main windings nor the secondary reactors involved in the process can be short-circuited. Those are the reasons of the careful delay carried out every tap change. Furthermore, it must be clarified that the tap change happens in the HV side of the transformer, in this case at the POC side of the wind farm. Firstly, it is surrounding the low-voltage winding, so accessing the auxiliary connections is easier. Secondly, in the HV winding there is lower currents, therefore lower electromechanical forces can be tackle with smaller and cheaper components.

3.2.1 Optimisation

In this second strategy, the wind farm voltage control is coordinated with the OLTC transformer. Still, the procedure for the optimisation problem within the MPC is the same as in Section 3.1.1. It consists of two modes and four elements as before, but the first element (controlled variables) adds up a new measurement of the current tap position: n_{tap} .

Secondly, the decision variables integrate a new parameter: Δn_{tap} . It is the tap position increment of the main transformer (OLTC) of the wind farm. According to the discrete characteristic of the machine, the variable is declared as an integer number.

Thirdly, the objective function remains unchanged, so equal to Equation (3.1). However, its three components integrate new elements related to tap changes. Regarding the prediction horizon T_p , it is now 10 seconds in order to hold the slow process of the tap transformer. Yet, T_c and ΔT_p are the same value as for the first strategy to integrate the fast changes of WTGs. The three components of the objective function are the following:

$$\Delta V_{POC}^{pre}(k) = V_{POC}(k) - V_{POC}^{ref} + \frac{\partial |V_{POC}|}{\partial Q_{WT}} \cdot \Delta Q_{WT}(k) \quad (3.12)$$

$$\Delta V_{MV}^{pre}(k) = V_{MV}(k) - V_{MV}^{ref} + \frac{\partial |V_{MV}|}{\partial Q_{WT}} \cdot \Delta Q_{WT}(k) + \frac{\Delta |V_{MV}|}{\Delta n_{tap}} \cdot \Delta n_{tap}(k) \quad (3.13)$$

$$\Delta V_{WT}^{pre}(k) = V_{WT}(k) - V_{WT}^{ref} + \frac{\partial |V_{WT}|}{\partial Q_{WT}} \cdot \Delta Q_{WT}(k) + \frac{\Delta |V_{WT}|}{\Delta n_{tap}} \cdot \Delta n_{tap}(k) \quad (3.14)$$

As it can be seen, Equation (3.12) is equal to Equation (3.2). It is because an electrical coupling is considered between the POC bus and the main bus of the external network. That means that the effect of a tap change is neglected in the HV side of the transformer. On the other side, Equation (3.13) and (3.14) include the new decision variable Δn_{tap} . Then, the effect of a tap change is indeed considerable for the rest of buses, assuming the POC bus as the reference k . Its multiplier corresponds to the voltage magnitude sensitivity to each tap step.

Fourthly, the same constraints (3.5) and (3.6) are considered. Moreover, the operational limits of the OLTC are included in. First, it only can change positions one by one. Second, the configuration range has 17 positions. These constraints are implemented as follows:

$$\begin{aligned} -1 &\leq \Delta n_{tap}(k) \leq 1 \\ -8 &\leq n_{tap}(k) \leq 8 \end{aligned} \quad (3.15)$$

Finally, a conditional and temporal limit (3.16) is created as security delay. In spite of the operational delay, an extra second limit ensures that the transformer is mechanically stabilised after a tap step and there is no risk of too many electrical contacts at the same time.

$$\Delta n_{tap}(k) = \begin{cases} \Delta n_{tap}(k), & \text{if } \sum_{k=t_0-5}^{t_0} \Delta n_{tap}(k) = 0 \\ 0, & \text{otherwise} \end{cases} \quad (3.16)$$

3.2.2 State Space Model

After the presentation of optimisation changes related to this second strategy, the modifications in the modelling part are going to be explained in this section. The system state space model keeps being the same as presented in Equation (3.7). However, its elements are modified in order to integrate the new decision variable Δn_{tap} . Firstly, the variables of the system are the following:

$$\begin{aligned} x &= [\Delta Q_{WT_1}, \dots, \Delta Q_{WT_{N_W}}, \Delta n_{tap}]^T \\ u &= [\Delta Q_{WT_1}^{ref}, \dots, \Delta Q_{WT_{N_W}}^{ref}, \Delta n_{tap}^{ref}]^T \\ y &= [\Delta Q_{WT_1}, \dots, \Delta Q_{WT_{N_W}}, \Delta n_{tap}]^T \end{aligned}$$

Where the new decision variable related to the OLTC of the output variable array y can be identified in Equations (3.13) and (3.14). Therefore, integrating also the input variable u and its tap reference into the minimisation process.

Next, the associating matrices holding the dynamics of the system elements are presented. Regarding WTGs, the model and A_{WT} , B_{WT} , C_{WT} matrices remain the same. On the other hand, the OLTC behaviour is introduced here. In the previous research work, the OLTC was automatically controlled by its automatic voltage regulator (AVR) as it is shown in Figure 3.2. However, now it is controlled by the MPC. Then, a tap position change in reference Δn_{tap}^{ref} is the input of the control system instead of voltage reference desired. Eventually, only the time-delay is modelled from the AVR reference.

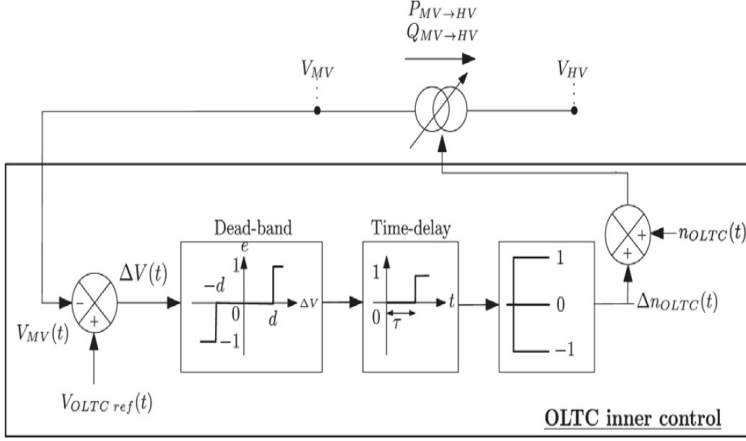


Figure 3.2: AVR control of a OLTC transformer [36]

Therefore, the mechanical delay of a change in internal connections is modelled as T_{tap} . What is considered as 5 seconds in this case. The state space model of the transformer is presented in Equation (3.17) as a dynamic model and in Equation (3.18) as an already discrete model due to its simplicity.

$$\Delta n_{tap} \dot{=} A_{OLTC} \cdot \Delta n_{tap} + B_{OLTC} \cdot \Delta n_{tap}^{ref} \quad (3.17)$$

$$\Delta n_{tap}(k) = \Delta n_{tap}^{ref}(k - T_{tap}) \quad (3.18)$$

3.3 Wind Farm + VSC-HVDC Voltage Control

HVDC technology is already widely spread since the first submarine cable was installed in Sweden in 1954. Some of its advantages are presented in [37]: lower investment cost from 50 km or longer cables, lower power losses, there is not reactive power generation such that in long AC cables, it can connect different synchronous systems and it allows controlling power parameters. However, it is getting more attractive because of two reasons. First, many offshore wind farms are being planned and HVDC is a solution for transmitting bulk power across long-distance submarine cables. Second, there are proposals of a DC-supergrids for European-level interconnection [38].

According to those challenges, the voltage sourced converter (VSC) technology was developed. Firstly, it offers fast and full controllability of the converter terminal, even AC active and reactive power independently. Secondly, it allows a multi-terminal

(MT) solution. Its main differences with the traditional HVDC-converter methodology [39] are: the use of bidirectional controlled thyristor and an inductive reactor between the converter terminal and the network. Besides, it still integrates the usual filters and DC capacitors. Furthermore, some more advantages are simple control, few harmonic generation, adjustable power factor and black up capability.

In spite of the wide use of the VSC technology, most of the literature is focused on the DC-voltage control for MT-grid control. For this reason and with a assumed DC-supergrid working as a slack bus and taking care of the DC-voltage, this project aims at controlling the AC-terminal of the VSC converter what would bring some benefits for the wind farm side terminal despite of the DC-link.

3.3.1 Optimisation

Along this third strategy, the coordinated device is the VSC of the wind farm side. As it is explained for the OLTC, the optimisation problem follows the structure presented in Section 3.1.1. Again, the controlled variables are the first part of the problem and they remain the same.

Secondly, a new decision variable comes up as ΔV_c . It states the voltage magnitude increment of the voltage-sourced converter (VSC) on the AC-terminal of the wind farm side. This new variable is added up to the ΔQ_{WT} array, but the Δn_{tap} is not considered any more.

Thirdly, the same objective function is defined according to Equation (3.1). The prediction horizon has the same value as in the first strategy, $T_p = 5seconds$. Since the VSC dynamics make fast effects, no more time is considered. Each of the three elements of the objective functions are presented here:

$$\Delta V_{POC}^{pre}(k) = V_{POC}(k) - V_{POC}^{ref} + \frac{\partial |V_{POC}|}{\partial Q_{WT}} \cdot \Delta Q_{WT}(k) + \frac{\partial |V_{POC}|}{\partial V_c} \cdot \Delta V_c(k) \quad (3.19)$$

$$\Delta V_{MV}^{pre}(k) = V_{MV}(k) - V_{MV}^{ref} + \frac{\partial |V_{MV}|}{\partial Q_{WT}} \cdot \Delta Q_{WT}(k) + \frac{\partial |V_{MV}|}{\partial V_c} \cdot \Delta V_c(k) \quad (3.20)$$

$$\Delta V_{WT}^{pre}(k) = V_{WT}(k) - V_{WT}^{ref} + \frac{\partial |V_{WT}|}{\partial Q_{WT}} \cdot \Delta Q_{WT}(k) + \frac{\partial |V_{WT}|}{\partial V_c} \cdot \Delta V_c(k) \quad (3.21)$$

Unlike Equation (3.12), Equation (3.19) takes into account the new decision variable. That is because the HVDC link decouples the wind farm from the main network, so every change in the VSC terminal makes a direct effect in every bus. Therefore,

Equations (3.19), (3.20) and (3.21) integrates the influence of ΔV_c . Its multiplier corresponds to the voltage magnitude sensitivity regards to the mentioned AC terminal, which is explained in Section 2.4 and its reference k bus corresponds to the POC bus.

Fourthly, constraints (3.5) and (3.6) are included again in this problem. At the same time, the AC-terminal of the VSC of the wind farm side is limited by the constraint which includes the voltage threshold at the POC bus.

3.3.2 State Space Model

Regarding this third strategy and the installation of the VSC-HVDC, it also makes some modifications in the modelling part. Based on the same state space model presented in Equation (3.7), the variables of the system must now include in the decision variable ΔV_c of the optimisation. The output variables array y can be found in Equations (3.19), (3.20) and (3.21) while all the variables are the following:

$$\begin{aligned} x &= [\Delta Q_{WT_1}, \dots, \Delta Q_{WT_{N_W}}, \Delta u_s^{d-ref}, \Delta u_s^d, \Delta u_{int}^d, \Delta i_{PI}^d]^T \\ u &= [\Delta Q_{WT_1}^{ref}, \dots, \Delta Q_{WT_{N_W}}^{ref}, \Delta V_s^{ref}]^T \\ y &= [\Delta Q_{WT_1}, \dots, \Delta Q_{WT_{N_W}}, \Delta V_c]^T \end{aligned}$$

Where ΔV_c and ΔV_s^{ref} are voltage magnitude increments at the VSC-terminal of the wind farm side and at the POC bus. It means between the two points of measurement are some losses modelled such as filters, phase reactor and internal elements. Losses represented by C_f in the following equations. On the other hand, the new state variables Δu_s^{d-ref} , Δu_s^d , Δu_{int}^d , Δi_{PI}^d are respectively voltage magnitude reference increment from the MPC, voltage magnitude measurement increment, an internal control voltage magnitude increment and current increment from the PI controller of the inner loop. All of them are referred to the parameter d , which states the d-axis from the dq-frame. Taking into account the following assumption: $V_s = \sqrt{(u_s^d)^2 + (u_s^q)^2} \approx u_s^d$.

Although WTGs elements are the same as presented in Sections 3.1.2 and 3.2.2, the VSC parameters must be explained with a control scheme. While a simplification suggested by [28] is shown in Figure 3.3, its parameters and the relationship with above variables are stated in the following transfer functions. First, the *Delay* block corresponds to a T_d first-order delay function in (3.22). Second, the *u_{AC}OuterLoop* corresponds to the PI controller (second term) within (3.25), with k_{o_p} as the proportional gain and k_{o_i} as the integral gain. Third, the *i_{dq}InnerLoop* is simplified as a T_{inr} simplified time constant of the inner control loop within (3.25)(first term). Fourth, the *PhysicalFilterModel* regards to the C_f capacitor filter in (3.23).

$$\Delta u_s^{d-ref} = \frac{1}{1 + s \cdot T_d} \cdot \Delta V_s^{ref} \quad (3.22)$$

$$\Delta u_s^d = -\frac{1}{s \cdot C_f} \cdot \Delta i_{PI}^d \quad (3.23)$$

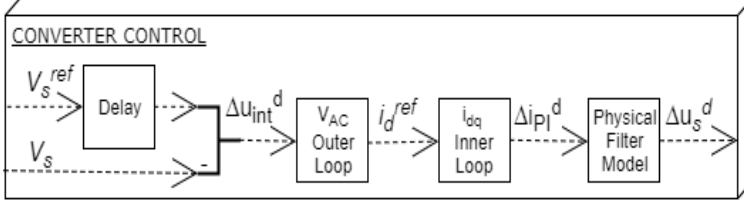


Figure 3.3: VSC Control Scheme

$$\Delta u_{int}^d = \frac{\Delta u_s^{d_ref} - \Delta u_s^d}{s} \quad (3.24)$$

$$\Delta i_{PI}^d = -\frac{1}{1 + s \cdot T_{inr}} \cdot \left(k_{o_p} + \frac{k_{o_i}}{s} \right) (\Delta u_s^{d_ref} - \Delta u_s^d) \quad (3.25)$$

Where

$$\begin{aligned} \Delta V_s^{ref} &= V_s^{ref} - V_s(t_0), \\ \Delta u_s^{d_ref} &= u_s^{d_ref} - u_s(t_0), \\ \Delta u_s^d &= u_s^d - u_s(t_0), \end{aligned}$$

and, all the values of these variables are shown in the following Table 3.1.

VSC Parameters	
Parameter	Value
C_f	10^{-6} F
T_d	0.1 sec
T_{inr}	0.005 sec
k_{o_p}	0.1
k_{o_i}	10

Table 3.1: VSC Parameters

To sum up, the VSC dynamic state space model shows like the following equation:

$$\begin{aligned} \dot{x}_{VSC} &= A_{VSC} \cdot x_{VSC} + B_{VSC} \cdot u_{VSC} \\ y_{VSC} &= C_{VSC} \cdot x_{VSC} \end{aligned} \quad (3.26)$$

Where $x_{VSC} = [\Delta u_s^{d_ref}, \Delta u_s^d, \Delta u_{int}^d, \Delta i_{PI}^d]'$, $u_{VSC} = [\Delta V_s^{ref}]$ and, $y_{VSC} = [\Delta V_c]$. Eventually, the associating matrices of the device are the following:

$$A_{VSC} = \begin{bmatrix} -\frac{1}{T_d} & 0 & 0 & 0 \\ 0 & 0 & 0 & \frac{1}{C_f} \\ 1 & -1 & 0 & 0 \\ -\frac{k_{o_p}}{T_{inr}} & -\frac{k_{o_p}}{T_{inr}} & -\frac{k_{o_i}}{T_{inr}} & -\frac{1}{T_{inr}} \end{bmatrix},$$

$$B_{VSC} = \begin{bmatrix} 1 \\ \frac{1}{T_d} \\ 0 \\ 0 \\ 0 \end{bmatrix},$$

$$C_{VSC} = \left(\frac{\partial |V_s|}{\partial |V_c|} \right)^{-1} [0, -1, 0, 0],$$

3.4 Power Factory

3.4.1 Wind Farm Voltage Control

As it is introduced at the beginning of this chapter, Power Factory is the tool for implementing the physical network and controllers. This project is developed over the so-called Nordic32 power system which can be seen in Figure 3.4. It is suggested by the IEEE as a benchmark for voltage stability and dynamic studies. Specifically, the voltage control analysis addresses a new offshore wind farm connected to bus 1042 of the Central grid.

A more accurate description of the wind farm topology is shown in Figure 3.5. There are 20 x 5 MW type-4 WTGs and an OLTC transformer, that for this first strategy it disables the AVR controller hence it is a common transformer with fixed tap position. In addition, the VSC-HVDC system is also disabled for this strategy.

Next, it is going to be explained the most important part of the Power Factory work. This is the voltage controller. It is implemented as an *ElmVol* slot within a frame. This frame provides a series of slots such as measurement of voltage buses, measurement of WTG power supply and the WTG machine indeed receiving references from the MPC voltage controller. Thus, working as an integrating interface for measurements, signals and devices of the topology previously mentioned.

Further details of the voltage controller are shown in Figure 3.6. There, the relationship between the controller and its signals can be seen on the left side. First, the measurements of voltage magnitude V_{WT} and voltage phase θ_{WT} for each of the 20 WTGs. The same parameters are measured for the three main buses of the wind

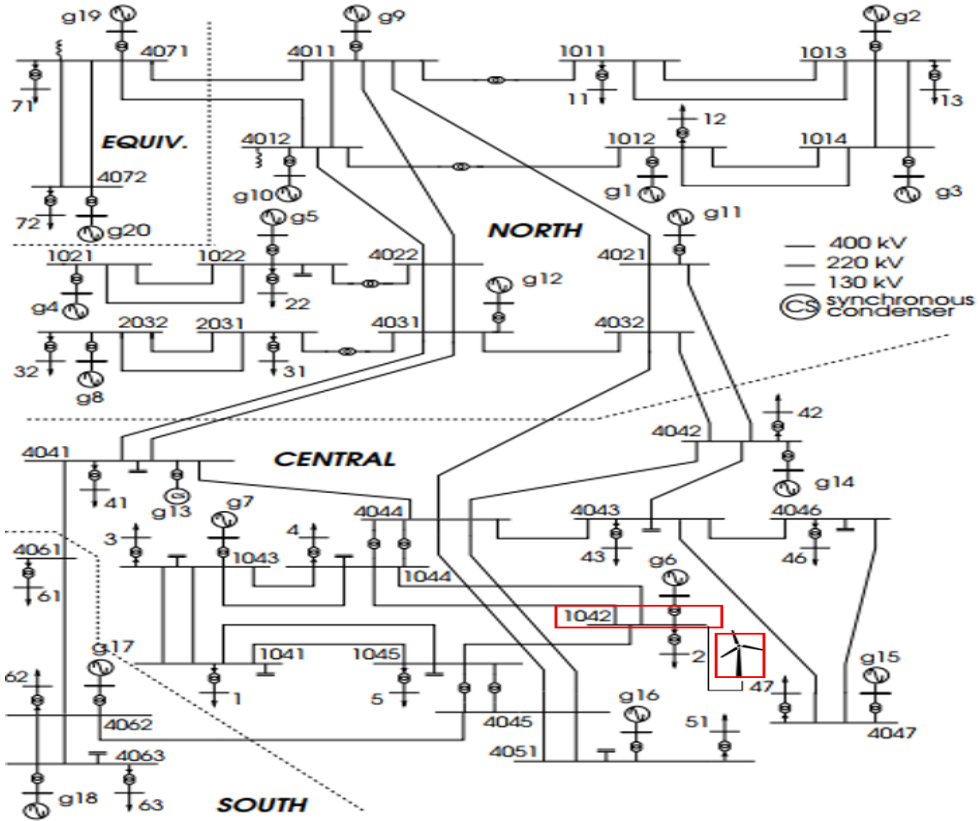


Figure 3.4: Nordic32 Power System [40]: Single-Line Diagram

farm: external bus 1042 V_{ext} , point of connection V_{POC} and medium-voltage bus V_{MV} . Moreover, current active and reactive power of each of the WTGs is also considered as an input: P_{WT} and Q_{WT} . Eventually, a variable with simulation time is calculated and communicated for the right interaction between the two softwares. On the other hand, the voltage controller output corresponds to the output of the MPC. In this strategy, this is an array with the reactive power reference Q_{WT}^{ref} of each of the WTGs.

Furthermore, its communication with Matlab is presented on the right side of Figure 3.6. There, a routine is run representing the whole MPC. In this case, each of the stages are organised as the process is developed. In conclusion, the Matlab MPC works as an embedded function within the voltage controller slot for the rest of elements of Power Factory frame.

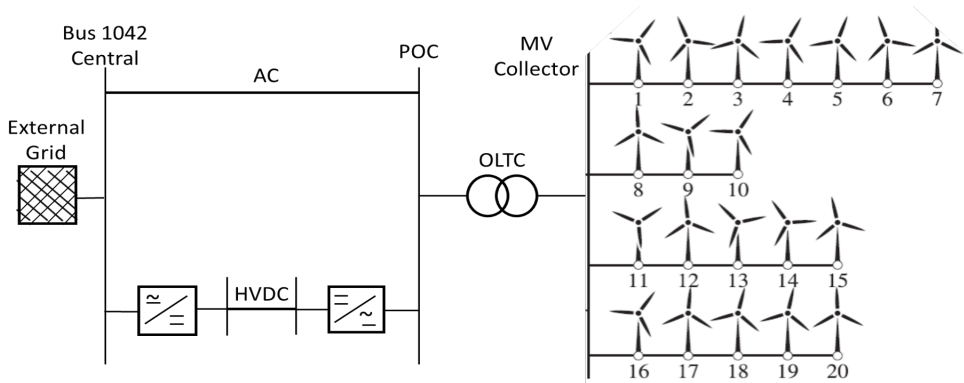


Figure 3.5: Wind Farm Network: Single-Line Diagram

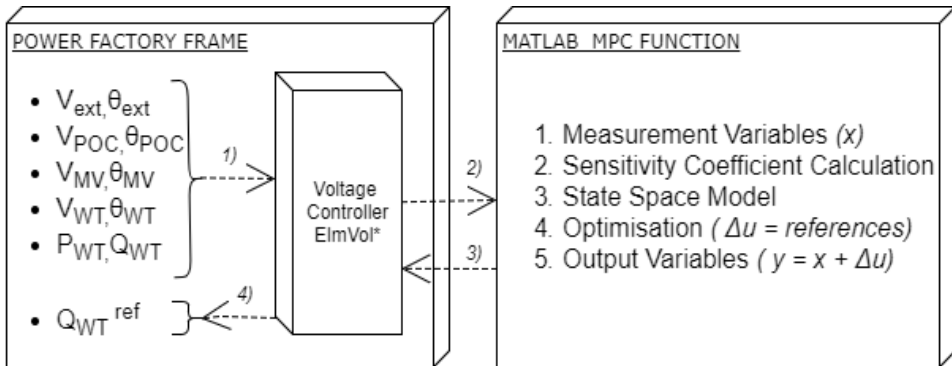


Figure 3.6: Voltage Controller Scheme

Finally, it is worth noting a WTG model implemented in Power Factory. A simplified example is shown in Figure 3.7. First, a slot represents the time-delay according to the transfer function explained in Equation (3.8). Second, the electrical machine is modelled as a variable load. Thus, an inversion of signs is needed for the output parameters. Regarding the input signals of the WTG, firstly Q_{WT}^{ref} comes from the Matlab MPC algorithm and provides the reference VAR output of the machine. Secondly, V_{WT} and θ_{WT} are the measurements from the network buses. Thirdly, P_{wind}^{av} states the available power in the wind limiting the electrical maximum output of the generator. These parameters will determine the operational behaviour of the wind turbine, hence providing the actual active P_{WT}^{ext} and reactive Q_{WT}^{ext} power supply.

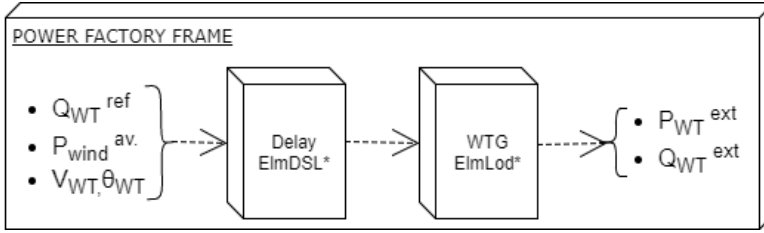


Figure 3.7: WTG Scheme

3.4.2 Wind Farm + OLTC Voltage Control

Based on the same system topology, the second voltage control analysis is addressed. Still, the OLTC AVR and the VSC-HVDC are out of service within the wind farm. Otherwise, the OLTC is now controlled by the MPC algorithm. Indeed, its optimal tap position n_{tap}^{opt} is updated according to the decision variable Δn_{tap} in Equations (3.13) and (3.14). A schematic representation is shown in Figure 3.8 laying down in the following expression: $n_{tap}^{opt} = n_{tap} + \Delta n_{tap}^{ref}$.

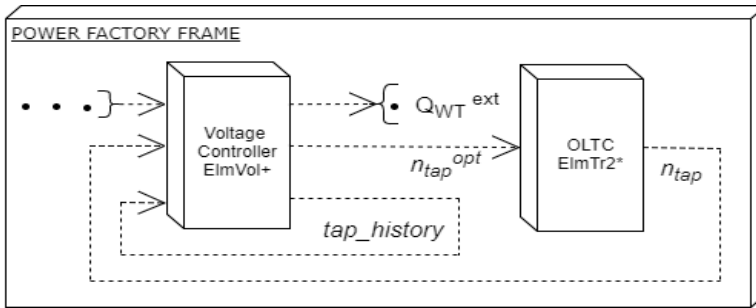


Figure 3.8: OLTC Scheme

Consequently, the voltage controller is updating the current measured tap position n_{tap} with the incremental tap step decided in the optimisation part of the Matlab MPC function. This current measurement comes from the OLTC slot which states the electrical machine displayed as an *ElmTr2* element. On the other hand, more signals can be found in the layout. First, the dotted input represents all the input measurements as they are in Figure 3.6. Second, the output reference for WTGs, which also remains the same. Third, the *tap_history* loop. This signal consists of a memory variable for next MPC iteration. It is an array which handles the last five tap position increments decided by the minimisation process. Thus, it carries out two functions. Firstly, the reminder checks out the constraint (3.16). Secondly, it performs the discrete machine model of Equation (3.18).

3.4.3 Wind Farm + VSC Voltage Control

Following the same procedure, the third voltage control is tested again in the Nordic32 system. However, the wind farm topology is now modified. The AC line is switched off and the DC system is operational in this case. Regarding the OLTC, both the AVR and the MPC control for this device are disabled hence a fixed tap position is set. However, the MPC takes over the wind farm VSC-terminal and WTGs as well. In this case, the voltage controller scheme corresponds to Figure 3.9. There are two output signals now. First, Q_{WT}^{ref} and second, a new reference for the voltage magnitude of the VSC terminal V_s^{ref} . This voltage reference comes from the following equation: $V_s^{ref} = V_{POC} + \Delta V_s^{ref}$. Where the former term is the current measurement and the latter comes from the MPC optimisation solution. It must be reminded that ΔV_s^{ref} is related to ΔV_c through the state space model in Section 3.3.2. Being this last variable, the one which appears in the objective function terms from Equation (3.19) to (3.21).

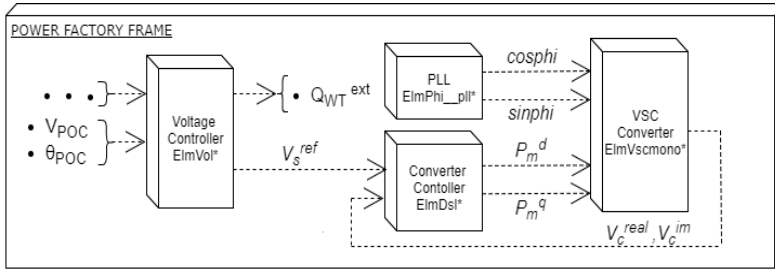


Figure 3.9: Wind Farm VSC Scheme

Regarding the rest of members in Figure 3.9, there are three new slots. First, the Phase Locked Loop (PLL) supplies reference signals $\cos\phi$ and $\sin\phi$ to the converter based on the frequency and phase of its input. These parameters are measured at *Bus1042 – CentralNetwork* with a synchronised oscillator. Second, the converter controller. It is receiving the reference V_s^{ref} and the measurement of the current voltage at the VSC terminal. Then, providing the modulation indexes P_m^d and P_m^q , that control the behaviour of the real converter. The former one comes from the control scheme showed in Figure 3.3 to control the AC-voltage. The latter one is set to zero, as its controlled parameters (active power or DC-voltage)[41] are not of interest. Third, the slot *VSCConverter* states the real power-electronics machine modelled in the wind farm network. A 300-MVA device rated at $130kV_{AC}$ and $225kV_{DC}$ working in a $V_{AC} - \theta$ control mode. On the other hand, the terminal connected to the external network works in $V_{DC} - Q$ mode.

3.5 Results and Discussion

An assessment of the voltage controllers is carried out in this section. Each of them is tested through a dynamic or root-mean-square (RMS) simulation in Power Factory. This test consists of a 100-second study in which a WTG power output variation is implemented. Each of the machines is working around their 4-MW of active power supply. Therefore, power oscillations from 74 to 78 MW can be seen as a WF output in Figure 3.10. The input data states available power in the wind, which was generated in SimWindFarm integrating wind field models of turbulences and wake effects. Although a bigger variation in power could have been studied, this specific range was chosen due to the limited reactive power supply of WTGs. VAR contribution which is challenged for being close to their maximum active power output, as it is shown in the capacity curve of a WTG in Figure 3.1.

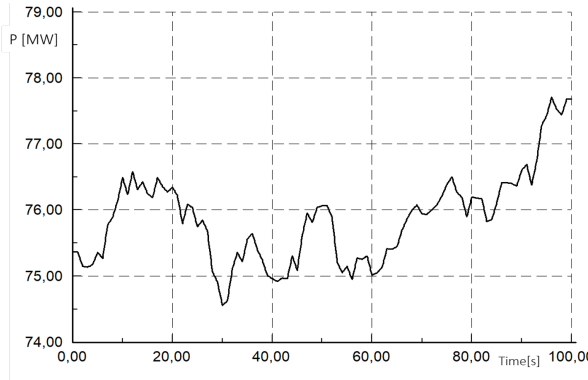


Figure 3.10: Wind Farm Active Power Output

3.5.1 Wind Farm Voltage Control

Aiming at a voltage profile improvement along the buses of the WF, this first strategy faces this main objective through the VAR supply of the WTGs. After a simulation, it can be highlighted that none of the nodes goes beyond their respective boundaries. That means that the voltage controller is all the time in *PreventiveMode* and hence, only the voltage magnitude at the POC bus is optimised every iteration. This allows a comparison of the results of each strategy focusing on the voltage profile at this bus: V_{POC} , which is illustrated in the upper part of Figure 3.11. Furthermore, the voltage magnitude at the MV bus V_{MV} is going to be analysed too and is shown in the lower part. It might state the behaviour of further WTG buses due to its direct relationship as a power collector.

It is clearly appreciable the improvement provided by the MPC optimisation. Along the simulation time in Figure 3.11 it minimises the voltage magnitude de-

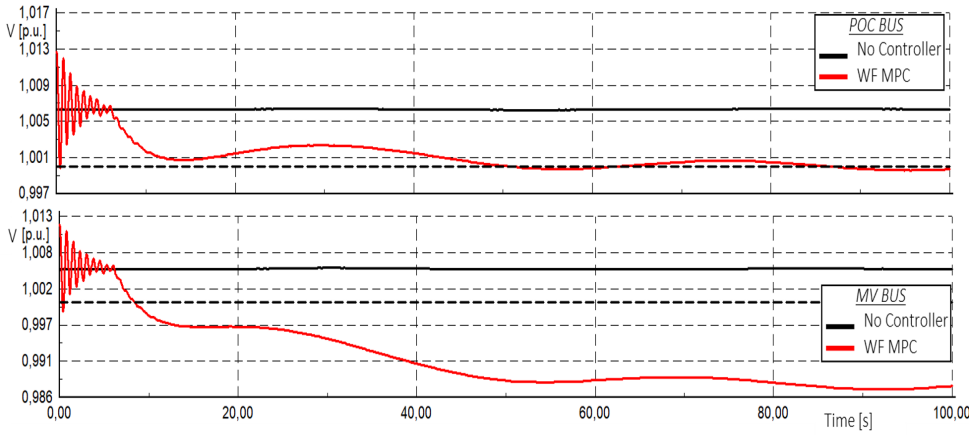


Figure 3.11: WFVC: Voltage Magnitude at POC and MV buses

viation from the bold-dashed reference at $V_{POC}^{ref} = 1p.u.$. Then, the absolute voltage error is reduced from $e_{POC}^{t5} = 0.006p.u.$ to $e_{POC}^{t100} = 0.0003p.u.$ at the last iteration. An interesting detail of the MPC can be pointed out. The control modelling part takes into account the dynamics of the generators and their time-delay response. Hence, avoiding an overshoot of the voltage wave after the control action takes over the VAR supply at $t_{sim} = 5s$. However, the MV bus voltage profile does not show such good improvement. Even more, its error increases from $e_{MV}^5 = 0.0051p.u.$ to $e_{MV}^{100} = 0.0128p.u.$. An error did not address by the MPC, since it is not included in the objective function of this operational mode. Nonetheless, it is reminded that is not go over its threshold set to $V_{MV}^{th} = 0.03p.u.$.

Finally, Figure 3.12 illustrate the behaviour of some representative WTGs. They are: WT1, WT7 and WT16 which are chosen for being the first and last generators of the longest feeder and, for belonging to the fourth feeder in the last case. Therein, the upper part shows a lower average deviation from the voltage reference. Even being almost zero for some of the machines. Thus, it states how the drop of voltage which was considered as a drawback for the MV bus brings an overall advantage for the WTG buses. Eventually, the reactive power response of those WTGs can be seen in the lower part. Their negative or absorbing behaviour help the machine nodes to fall their respective voltages. This approach represents until $1.406MVAr$ of inductive reactive power from the load perspective in the WT1 case.

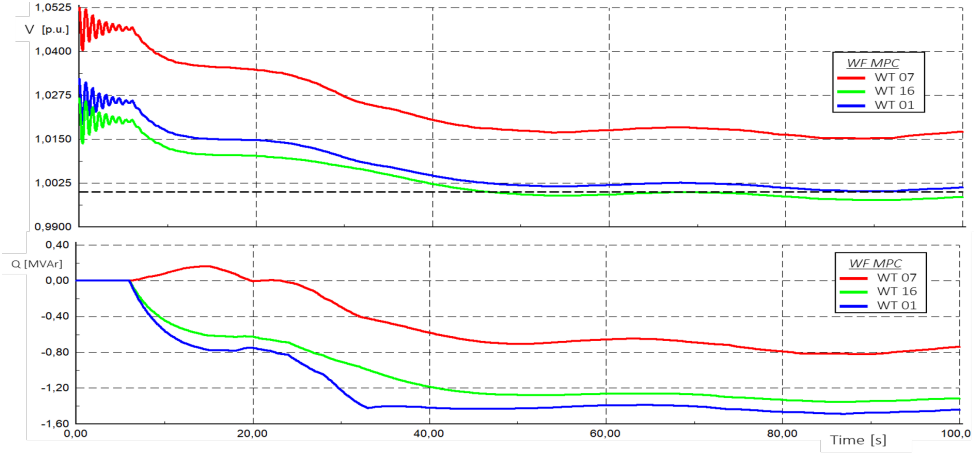


Figure 3.12: WFVC: Voltage Magnitude and Reactive Power of WTGs

3.5.2 Wind Farm + OLTC Voltage Control

Secondly, it is going to be explained how the control of an OLTC transformer upgrades the voltage evolution along the simulation. Again, the *PreventiveMode* prevails along the simulation and so, the V_{POC} is the main target to care about. This magnitude and V_{MV} are illustrated in Figure 3.13. Since in the previous simulation the MV boundary was not even close, this time and on $V_{MV}^{th} = 0.01 p.u.$. Hence, tighten constraints will challenge more the system. As it can be noticed, the V_{POC} variable performs exactly the same as in the case without OLTC. This is because of two reasons. First, the POC bus is coupled to the external network. Therefore, small changes within the WTGs contribution does not make a considerable influence. Second, the same coupling makes an OLTC tap change to modify only the voltages downwards itself. Therefore, the rest of WF buses suffers a modification. Regarding the tap change, this is a control action from the MPC in order to avoid the boundary now set at 0.99 p.u.. Firstly, it means a considerable improvement for the MV bus since it reduces the voltage deviation. The absolute error at $t = 100s$ reaches $e_{MV}^{OLTC} = 0.0001 p.u.$ regarding an initial $e_{MV}^{Init} = 0.0051 p.u.$ and $e_{MV}^{WFVC} = 0.0128 p.u.$ for the strategy *WFVC*.

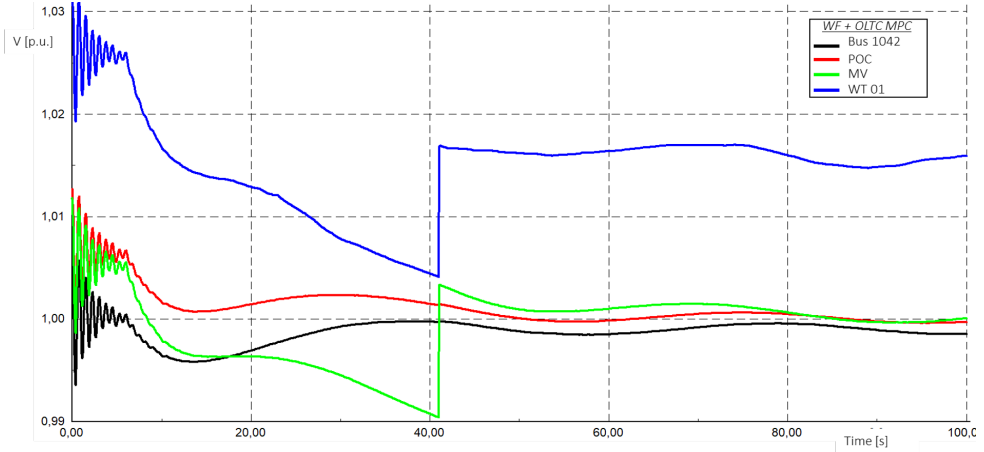


Figure 3.13: WF+OLTC VC: Voltage Magnitudes

Secondly, another modification is generated in the rest of WTG buses. The voltage step moves away all the magnitudes from their respective reference. This makes a worse situation for all the WTG nodes. This voltage change in some representative nodes can be seen in Figure 3.14. Moreover, the reactive power change from the *WFVC* strategy is shown too. There, it can be observed how the voltage step forced by the system pulls also the reactive power. What it is counteracted afterwards by the MPC control.

Further detail of the tap change is illustrated in Figure 3.15. The decision variable ΔN_{tap} from the MPC optimisation is shown there. Reminding that this variable must be discrete according to the transformer characteristics, a filter must be applied to this decision variable. Consequently, only a tap change is carried out over a certain threshold $N_{tap}^{th} = 0.75$. In the detail section within the figure is shown how a tap-down step (solid line) is applied at $t = 41s$, exactly $T_{tap} = 5s$ after the decision variable overtakes the red boundary.

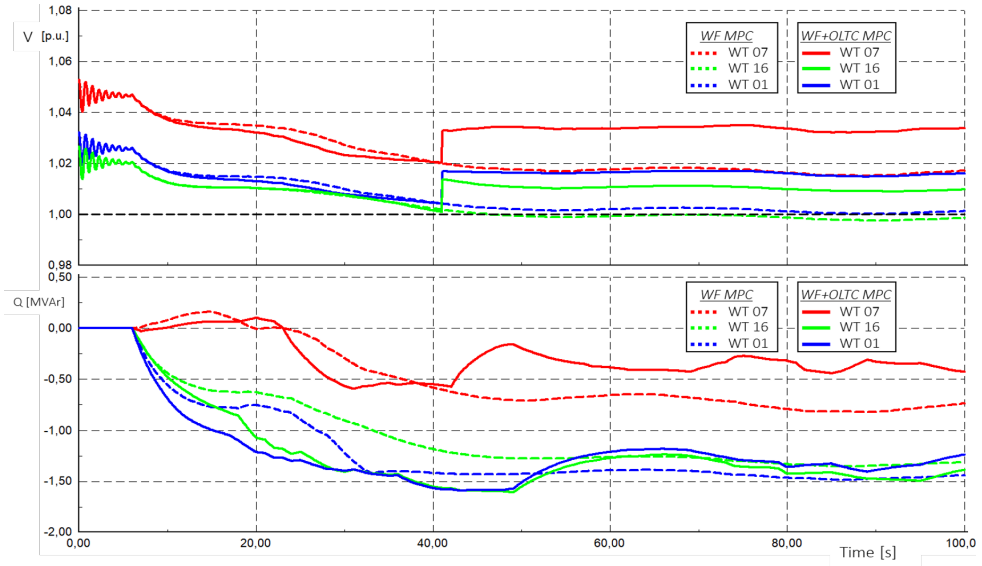


Figure 3.14: WTGs: Voltage Magnitude & Reactive Power

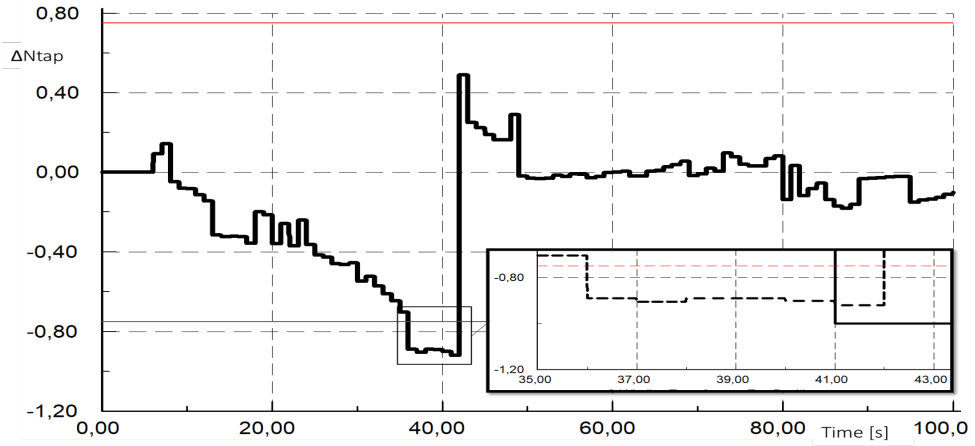


Figure 3.15: WF+OLTC VC: OLTC Tap Change Detail

3.5.3 Wind Farm + VSC Voltage Control

Thirdly, the controllability of the WF-VSC terminal is studied in this simulation. The AC voltage magnitude control provides further improvements which are illustrated in Figure 3.16. Therein, the V_{POC} and V_{MV} are shown and their absolute errors must be analysed for further comparison with the other strategies. Firstly, the error at $t = 100\text{s}$ is now $e_{POC}^{VSC} = 0.0003\text{p.u.}$ while it was $e_{POC}^{Init} = 0.006\text{p.u.}$ and $e_{POC}^{WFVC} = e_{POC}^{OLTC} = 0.0003\text{p.u.}$. Secondly, for the other bus is $e_{MV}^{VSC} = 0.0009\text{p.u.}$ while it was $e_{MV}^{Init} = 0.0051\text{p.u.}$, $e_{MV}^{WFVC} = 0.0128\text{p.u.}$ and $e_{MV}^{OLTC} = 0.0001\text{p.u.}$. Thus, getting with the VSC the same steady deviation in the POC bus and a worse steady value in the MV, according to the OLTC results.

Further detail of the VSC behaviour is illustrated in Figure 3.17. First, it appears the active power output of the WF which is injected into the converter. It is directly related to the V_{VSC}^{DC} variable of the HVDC-link, which is shown in the second part of the illustration. Therein, it is compared to $V_{VSC}^{AC} = V_{POC}$ and to V_{MV} . Furthermore, V_{POC} is controlled by the converter and hence, it is directly influencing the reactive power supply by the converter in the third part of the illustration.

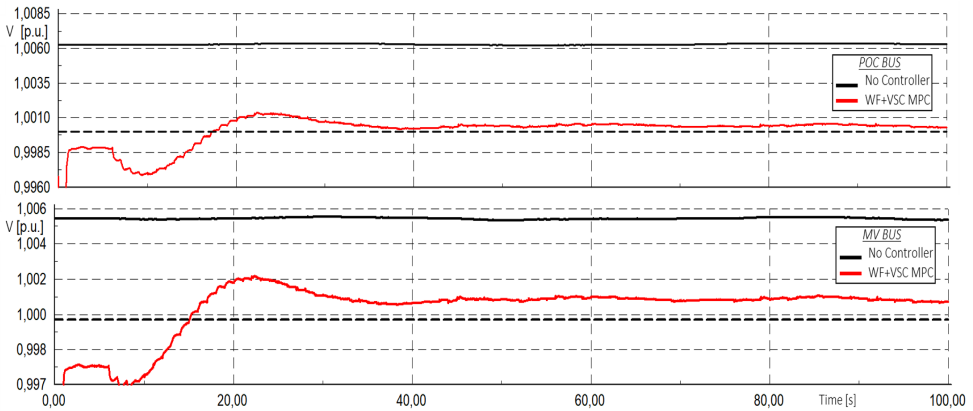


Figure 3.16: WF+VSC VC: Voltage Magnitude at POC and MV buses

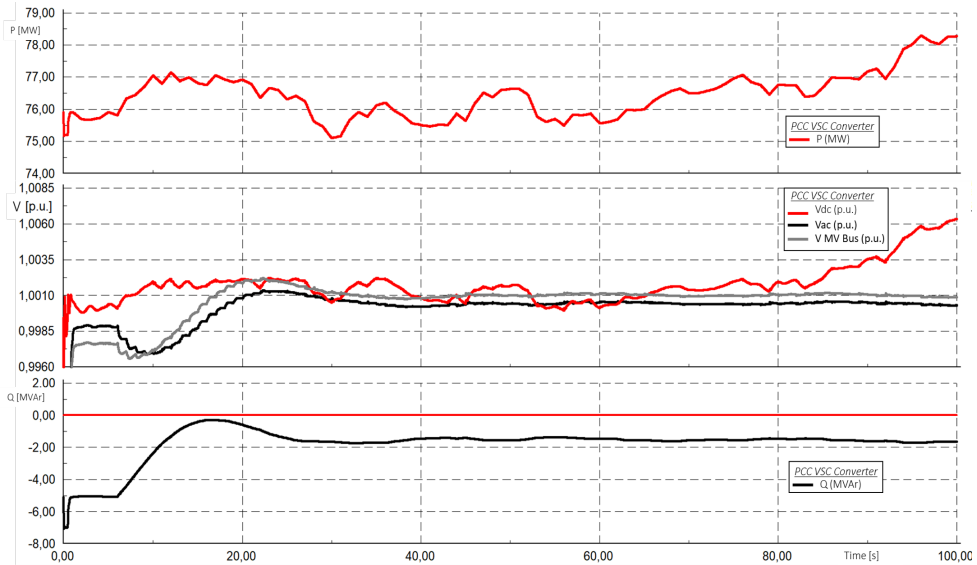


Figure 3.17: WF+VSC VC: VSC WF-Terminal Outputs

3.5.4 Discussion

Summing up, the three voltage controllers based on MPC enhance the voltage profile at the POC. Consequently, a good performance of the MPC can be acknowledged, since that node was mainly covered by the objective function. Moreover, when two of those, the OLTC and the VSC, manage a decision variable the MV bus also gets an enhancement. These two facts are summarised in Figure 3.18.

On the other hand, the rest of nodes in the WF do not follow the same accuracy to the reference. Still, all the magnitudes are within safe limits. Besides, the three strategies get an improvement from the initial simulation without voltage control. Regarding these WTG buses, the best performance is achieved while controlling only the WTG VAR response (WT MPC). An overall analysis is illustrated in Figure 3.19 through the maximum and minimum voltage magnitude level for each controller. Therein, the WFVC or WF MPC gets the reference magnitude between its two WTG voltage levels. Therefore, ensuring all the other voltages in between and hence, the average range of voltages is closer to $V_{WT}^{ref} = 1p.u..$

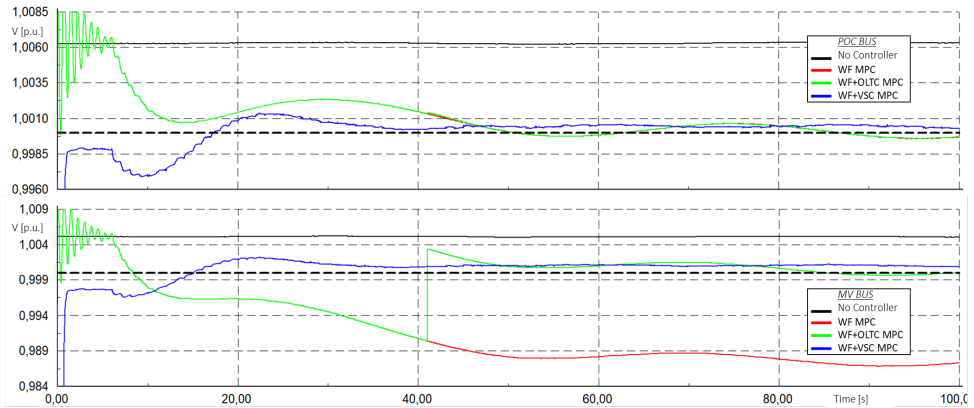


Figure 3.18: VC Comparison: Voltage Magnitude at POC and MV buses

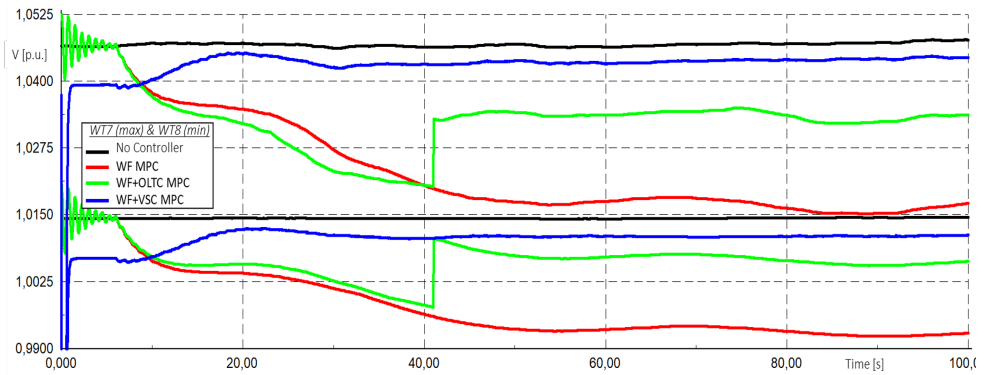


Figure 3.19: VC Comparison: WT7 and WT8 Voltage Magnitudes

A more accurate analysis of the results is shown in Table 3.2. The previous arguments were based on the absolute error at 100 seconds of simulation, assuming an steady state of the magnitudes. Nonetheless, this table gathers also the mean squared error (MSE) or quadratic error along the simulation from the initial action at 5 seconds to the last iteration at 100 seconds with time steps of 0.01 seconds.

VC Error Comparison			
Voltage Control	Absolute POC Error $e_{POC}^{t_{100}}$ (p.u.)	Absolute MV Error $e_{MV}^{t_{100}}$ (p.u.)	MSE POC Error ε_{POC}^2 (p.u.)
No Contr.	0.0060	0.0051	3.9542×10^{-5}
WF	0.0003	0.0128	2.1790×10^{-6}
WF+OLTC	0.0003	0.0001	2.1845×10^{-6}
WF+VSC	0.0003	0.0009	8.9076×10^{-7}

Table 3.2: Voltage Controller Error Comparison

Consequently, the following comments can conclude this study. According to the absolute error at the POC, any of the controllers bring an excellent performance. Then, the absolute error at the MV bus might be a decision aspect since the best behaviour is found in the WF+OLTC voltage control strategy. Otherwise, the MSE suggests that the lower error and hence, the best controller is the WF+VSC. To conclude, the final decision is accepting the WF+VSC voltage control strategy as the best one and so, implementing it in further studies. This decision is made according to four reasons. First, the MSE is considered more important since it takes into account the whole simulation time. It means a faster error minimisation. Second, the MSE states the objective function of the MPC optimisation. Thus, it respects strictly the target set at the beginning of the study. Third, the difference between the two last strategies in regards to the absolute error at the MV bus is considered as acceptable. Fourth, the VSC-HVDC technology is more attractive for future multiterminal DC networks from a subjective point of view.

CHAPTER 4

Network Coordination

4.1 Wind Farm + External OLTC Voltage Control

Once different technologies have been tested within the wind farm, it is time to try to coordinate them when they are installed outside the wind farm, i.e. in the main network. In this way, addressing the second challenge introduced in the objectives. Then, aiming at getting some voltage benefits also in external buses of the system.

Based on the comparison analysis carried out in previous chapter, the wind farm topology is set through the VSC-HVDC technology connected to *Bus1042 – CentralNetwork*. Meanwhile, an OLTC transformer in *CentralNetwork* is going to be controlled too. Therefore, coordinating both technologies for two purposes. First, keeping an optimal voltage level within the offshore grid. Second, improving the voltage profile of a close area to which the wind farm is connected.

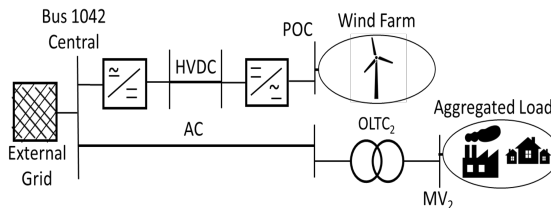


Figure 4.1: External Distribution Network: Single-Line Diagram

The OLTC installation is based on an approach to active management of grids with distributed energy resources (DER). Voltage variability would be produced due to the weather changing conditions affecting generation and energy storage systems. Then, this kind of network is assumed as connected to *Bus1042 – CentralNetwork*, as it can be seen in Figure 4.1. Modelling variability issues is carried out by a variable load along the time, following a consumption pattern from household demands. As voltage control is the target, a major role is given to the reactive power demand for creating voltage variations. While a static load is set as 50 MW and 50 MVar, the variable part of this load is following a profile with 70 MVar of maximum capacity. This profile can be seen in Figure 4.2 once is connected at 40 seconds.

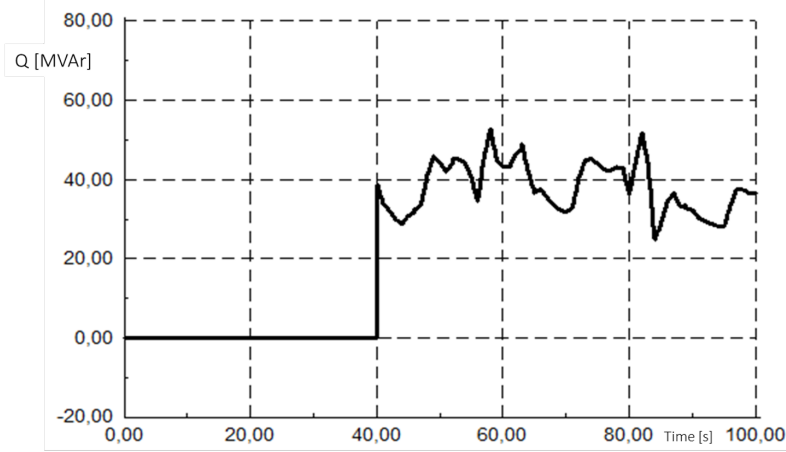


Figure 4.2: Variable Load:VAR consumption

4.1.1 Optimisation

This network coordination is carried out within the same voltage control framework as the previous chapter. The controller is based on a MPC algorithm, and this algorithm output depends on an optimisation which is subdivided in four parts. Nonetheless, this controller handles now the reactive power supply of the WTGs, the voltage magnitude of the WF-VSC-terminal and the new aggregated external $OLTC_2$ tap position. The following lines explain the parts of the MPC optimisation that integrate these three kind of devices.

Firstly, the parameters of which the MPC takes care of are called measured variables. There are two indices: V_{POC} is the voltage magnitude at the POC bus of the WF and V_{MV2} is the voltage magnitude at the MV bus of the external distribution network shown in Figure 4.1. The first one is chosen because the system operator gives its reference, hence it is the most important bus of the WF from the system point of view. The second parameter is decided as target because of its importance to downstream distribution consumers. Regarding their values, both references V_{POC}^{ref} and V_{MV2}^{ref} are set to $1p.u.$ and, their thresholds are $V_{POC}^{th} = 0.01p.u.$ and $V_{MV2}^{th} = 0.02p.u..$

Secondly, the decision variables of the optimisation set the references for the devices managed by the controller. As it is mentioned before, there are three kind of devices and so, three kind of decision variables. First, the incremental ΔQ_{WT} array of the 20 WTGs. Second, the change ΔV_c of the VSC. Third, the tap step of the external OLTC Δn_{tap} .

Thirdly, the objection function (4.1) tries to minimise the voltage error of the measured variables to their respective references. The same function is applied as in the previous optimisation sections. However, there are only two predicted error terms (4.2) and (4.3) within it, related to the two measured variable presented above. The long-term deviation is considered with N_p predicted steps coming from a prediction horizon $T_p = 10seconds$ and a prediction period $\Delta T_p = 0.5seconds$.

$$\min_{\Delta Q_{WT}, \Delta V_c, \Delta n_{tap}} \sum_{k=1}^{N_p} (\|\Delta V_{POC}^{pre}(k)\|^2 + \|\Delta V_{MV2}^{pre}(k)\|^2) \quad (4.1)$$

$$\Delta V_{POC}^{pre}(k) = V_{POC}(k) - V_{POC}^{ref} + \frac{\partial |V_{POC}|}{\partial Q_{WT}} \cdot \Delta Q_{WT}(k) + \frac{\partial |V_{POC}|}{\partial V_c} \cdot \Delta V_c(k) \quad (4.2)$$

$$\Delta V_{MV2}^{pre}(k) = V_{MV2}(k) - V_{MV2}^{ref} + \frac{\Delta |V_{MV2}|}{\Delta n_{tap}} \cdot \Delta n_{tap}(k) \quad (4.3)$$

Where all the terms have been introduced above and the partial derivatives corresponds to the sensitivity coefficients explained in Section 2.4. Respectively, the sensitivity to VAR response is calculate in Equation (2.8), the sensitivity to VSC-voltage change in Equation (2.14) and the sensitivity to tap changes in Equation (2.15). Nevertheless, it must be highlighted their reference k bus for the calculation. In spite of the fact that for the whole project and for the coefficients in (4.2) this bus is the POC bus of the WF, the new external distribution network make them change. Thus, the new network Y_{bus_2} must be considered in (4.3). Its new k reference bus is the bus HV-side of the new $OLTC_2$.

Fourth, the problem is constrained by the physical limits of network devices. To sum up, the following equations gather all ones already mentioned. Where WTG reactive power limits are in (4.4) and the transformer operational limits are in (4.5) to (4.7).

$$Q_{WT_i}^{min}(k) \leq Q_{WT_i}(k) \leq Q_{WT_i}^{max}(k) \quad (4.4)$$

$$\forall i \in [1, 20], \quad k \in [1, N_p]$$

$$-1 \leq \Delta n_{tap}(k) \leq 1 \quad (4.5)$$

$$-8 \leq n_{tap}(k) \leq 8 \quad (4.6)$$

$$\Delta n_{tap}(k) = \begin{cases} \Delta n_{tap}(k), & \text{if } \sum_{k=t_0-5}^{t_0} \Delta n_{tap}(k) = 0 \\ 0, & \text{otherwise} \end{cases} \quad (4.7)$$

4.1.2 State Space Model

The second part of the MPC algorithm consists of defining the network dynamics in order to integrate them into the previous optimisation. The dynamic behaviour of each of the elements controlled by the MPC has already been introduced in the previous chapter. However, their equations are summarised below for a good comprehension. Further details are already explained in the *StateSpaceModel* Sections before. First, the system continuous state space model is the following:

$$\begin{aligned}\dot{x} &= A \cdot x + B \cdot u \\ y &= C \cdot x\end{aligned}\tag{4.8}$$

Where their variables integrate now the three kind of devices in charge of the voltage control. Thus, appearing as decision variables in Equations (4.2) and (4.3). They are described as follows:

$$\begin{aligned}x &= [\Delta Q_{WT_1}, \dots, \Delta Q_{WT_{N_W}}, \Delta n_{tap}, \Delta u_s^{d-ref}, \Delta u_s^d, \Delta u_{int}^d, \Delta i_{PI}^d]^T \\ u &= [\Delta Q_{WT_1}^{ref}, \dots, \Delta Q_{WT_{N_W}}^{ref}, \Delta n_{tap}^{ref}, \Delta V_s^{ref}]^T \\ y &= [\Delta Q_{WT_1}, \dots, \Delta Q_{WT_{N_W}}, \Delta n_{tap}, \Delta V_c]^T\end{aligned}$$

Later on, the associating matrices of the system A , B and C are described individually for each of machine. First, the WTG dynamics are the following: $A_{WT}^i = \frac{-1}{T_{WT}}$ and $B_{WT}^i = \frac{1}{T_{WT}}$. Then, developing them for the machines of the whole system are:

$$\begin{aligned}A_{WT} &= \text{diag}(A_{WT}^1, \dots, A_{WT}^{N_W}) \\ B_{WT} &= \text{diag}(B_{WT}^1, \dots, B_{WT}^{N_W}) \\ C_{WT} &= \text{diag}(1_1, \dots, 1_{N_W})\end{aligned}$$

Second, the VSC behaviour is gathered in matrices A_{VSC} , B_{VSC} and C_{VSC} in Page 31.

Third, the $OLTC_2$ is represented by the following discrete equation due to its simplicity. Consequently, substituting the general continuous model (4.8), which will be discretised afterwards for the optimisation calculation.

$$\Delta n_{tap}(k) = \Delta n_{tap}^{ref}(k - T_{tap})\tag{4.9}$$

4.2 Power Factory

The network topology design is carried out in PowerFactory as it is stated before. The whole system Nordic32 and the controlled wind farm are illustrated in Figures 3.4 and 3.5. The new distribution grid with the variable load is design according to Figure 4.1. Then, it is connected to *Bus1042 – CentralNetwork*. Next, the voltage control explained in Section 4.1 is illustrated on the scheme in Figure 4.3. Therein, the

voltage controller included in a PowerFactory frame manages the WTGs, the external $OLTC_2$ and the WF-VSC. Consequently, the coordinated strategy is implemented.

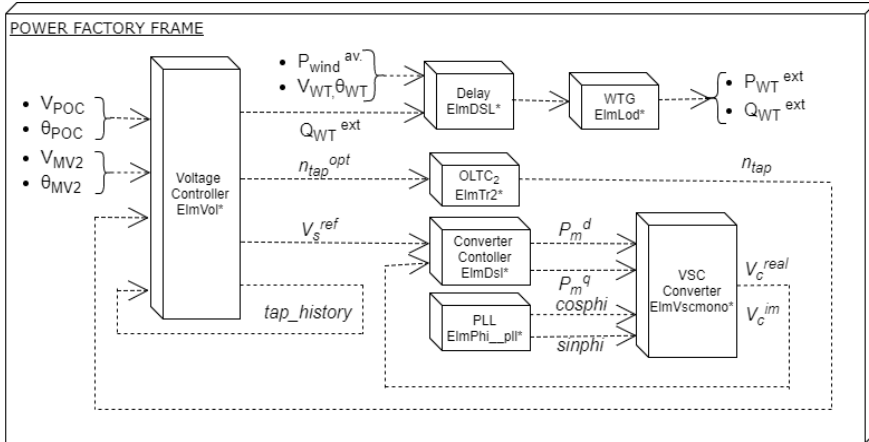


Figure 4.3: Voltage Control Scheme

4.3 Results and Discussion

The last coordinated voltage controller is going to be tested following the same procedure as for the WF alone. This is through a 100-second RMS simulation in Power Factory. An active power variation challenges the performance of the control strategy for assessment. This power variation is the same as introduced before in Figure 3.10. Moreover, the consumption load also implies an impact at the *Bus1042* in comparison to the case without variable load. This considerable effect in the reference bus is illustrated in Figure 4.4.

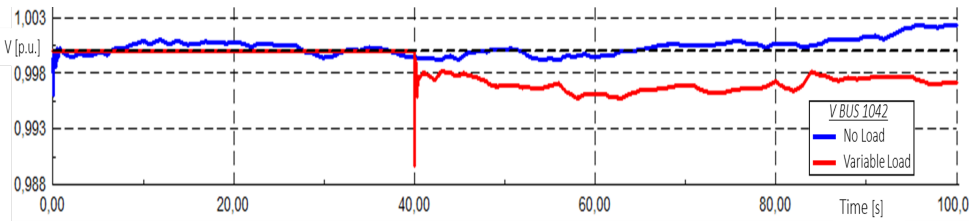


Figure 4.4: Voltage Impact in Bus 1042 due to Variable Load

Furthermore, this negative impact is expanded along the network. Then, challenging the wind farm too. As it is illustrated in Figure 4.5, the main bus voltages are threaten from the upper boundary to the lower one without any controller taking over the voltage control within the WF. On the other hand, the MPC handling the WTGs and VSC stabilises the voltage profiles around the 1 p.u. reference. Nonetheless, a little oscillation is observed along the rest of simulation together with some voltage peaks due to the tap steps in the external network.

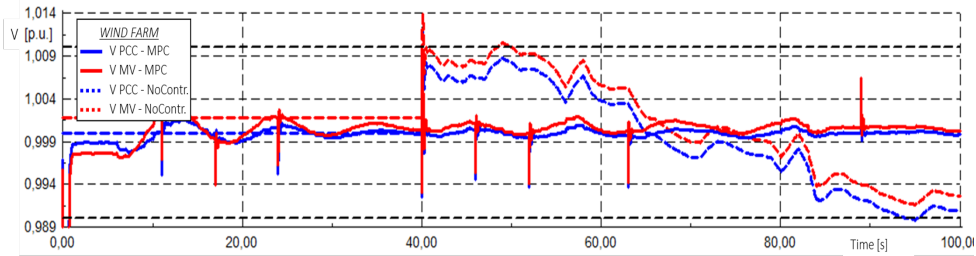


Figure 4.5: Voltage Profile within the WF

On the other hand, the behaviour of the voltage profile on the external grid can be analysed in Figure 4.6. Therein, the main buses of this network are represented and they are compared in two scenarios: without and with MPC controller. Due to the external network coupling, it can be seen how the main impact of the variable load points out at the LV-side (MV_B) of the OLTC transformer and not to the HV-side (PCC_B). Besides, the same coupling makes every tap change affect directly that MV-side. Thus, a perfect situation comes up for tackling the load variability and pull it within limits.

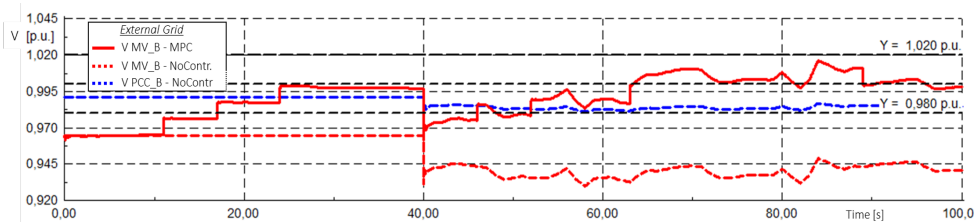
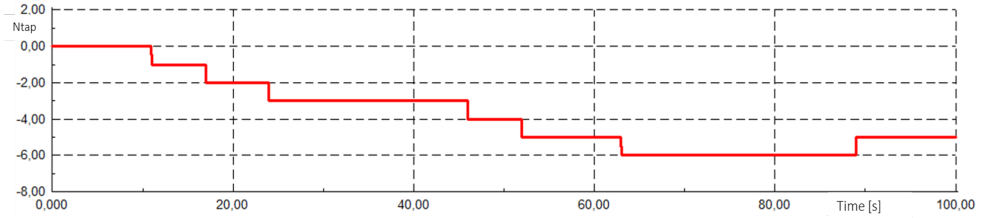


Figure 4.6: Voltage Profiles of Variable Load Network

Finally, the behaviour of the tap transformer in the external network is illustrated in Figure 4.7. In spite of the quick changes implemented in the load profile to challenge the network, there are enough tap changes for voltage improvements. These tap steps help the MV bus to stay within its threshold most of the time. It must be highlighted that the improvements are possible thanks to the three initial steps before the variable load is connected, time which was needed for a proper VSC stabilisation to deal with

Figure 4.7: Tap Position of $OLTC_2$

the fast changes. However, the slow dynamics of this device are present. Then, a perfect behaviour can not be achieved. Although an ideal voltage profile is not achieved, the improvements of handling the OLTC are shown in Table 4.1. In this case, the absolute error is dismissed due to the fast and constant changes of the VAR load profile. Then, the mean squared error brings a more accurate idea of the performance in comparison to the quadratic error objective function. This MSE is calculated from $t = 40s$ in advance, in order to focus on the voltage deviation once the variable load is switched on.

VC Error Comparison	
Voltage Control	MSE MV_2 Error $\varepsilon_{MV_2}^2$ (p.u.)
No Contr.	3.600×10^{-3}
MPC	1.516×10^{-4}

Table 4.1: Voltage Profile Error Comparison

Eventually, a proposal for keeping the voltage profile tighten to its reference might consists of faster VAR devices such as SVC or power-electronic converters like the VSC previously studied. Nonetheless, the fast VAR consumption profile implemented is only an example for challenging the grid. Since consumption patterns does not change that fast and they can be forecasted with certain accuracy, an OLTC is considered yet as a good voltage control device for distribution networks.

CHAPTER 5

Conclusion

In this project a wind farm voltage control is developed according to an MPC methodology. With voltage error minimisation as main objective, it points out at the POC bus first and the rest of wind farm buses as secondary target. Then, improving the voltage profile in the whole grid. Three MPC strategies are established. In each of them there is a voltage control coordination with different devices like WTGs, an OLTC and a HVDC-VSC for wind farm improvements. In spite of the different technologies, each strategy is explained in detail for an optimisation problem implementation. Covering input variables, decision variables, objective function and constraints for each case. Moreover, a state space model gathering the dynamics of each device is addressed. Modelling part that allows a future system state estimation and hence, a long-term voltage deviation minimisation. These predicted voltage errors are based on the integration of time-horizon system states and their effects on the network through voltage sensitivities. Coefficients which are calculated working out an analytical method.

Next, each of the strategies are assessed through an RMS simulation in PowerFactory. The results show a better behaviour at the POC bus in the three strategies in comparison to the base case without controller. Moreover, the OLTC and the VSC bring more benefits for the MV bus even though it was not the main target. Furthermore, the VSC provides a fast error reduction and so, the minimal MSE error. For this reason, it is considered the best strategy for voltage stability. On the other hand, the best voltage profile is found in the WTG buses when only their converters are controlled. Nonetheless, they are always within safety ranges hence this parameter is considered less decisive for choosing the best strategy. Once a successful behaviour in the wind farm is demonstrated, the MPC controller integrates an external OLTC transformer. This coordination allows keeping the wind farm buses in optimal performance while enhancing the voltage level in a variable load bus. Therefore, it is proved that a wind farm MPC voltage controller can effectively coordinate elements of an external grid for improving both grids.

In conclusion, the MPC technique works perfectly for power system coordination. In this case, the voltage target is achieved with optimal control actions joining different technologies. Its predictions together with an effective sensitivity provides an excellent performance for the wind farm studies carried out.

5.1 Future Work

As a continuation of the current work developed, a series of ideas are of interest for future studies. First, the robustness of each technology might be analysed. Although a good performance is achieved with each strategy, a more challenging scenario would be more interesting, for instance a low voltage ride through (LVRT) study. Second, further development in network coordination is affordable. This project present a controller coordinating several technologies of two networks but not a contribution for a common objective. For instance, both grids could support together the voltage level of the main external bus in common. Third, a multiterminal MT-HVDC system is missing. Next steps will consist of including more VSC terminals in the network, connecting different and far away areas. In this context, a coordination for voltage control purposes would be addressed. However, it would be focused on an MPC controlling the AC VSC terminals in contrast to the wide literature covering the DC-link voltage control.

CHAPTER 6

Conclusiones

En este proyecto se ha desarrollado un controlador de voltaje para un parque eólico basado en la metodología MPC (Controlador de Modelo Predictivo). Siendo el objetivo principal minimizar el error en el voltaje, el controlador se centra en primer lugar en el nodo POC y de forma secundaria en el resto de nodos del parque eólico. Así pues, mejorando el voltaje en toda la red. Para ello, se establecen tres estrategias con tres controladores MPC diferentes. Cada uno de ellos consiste en controlar el voltaje coordinando diferentes dispositivos como el generador de las turbinas (WTG), el ratio del transformador (OLTC) y el convertidor del sistema de corriente continua (HVDC-VSC). A pesar de las diferentes estrategias, cada una es explicada en detalle con el objetivo de implementar un problema de optimización. Dicho detalle consiste en variables de entrada, variables de decisión, función objetivo y restricciones para cada uno de los casos. Además, se introduce el modelo espacio-estado representando el comportamiento dinámico de cada uno de los dispositivos. Modelo que permite estimar el estado futuro de un sistema y por lo tanto, minimizar la desviación del voltaje a largo plazo. Estas predicciones del error del voltaje se llevan a cabo mediante el cálculo analítico de coeficientes de sensibilidad. Dichos coeficientes permiten integrar el estado de un sistema durante un periodo de tiempo junto con sus efectos en la red.

A continuación, cada una de las tres estrategias son evaluadas mediante una simulación dinámica (RMS) en el software PowerFactory (DigSilent). Los resultados muestran un mejor comportamiento en el nodo POC en los tres casos, en comparación con el caso básico sin controlador. Además, el transformador OLTC y el convertidor VSC permiten obtener más beneficios en el nodo MV, incluso sin ser este segundo nodo el objetivo principal. Aún más, el convertidor VSC proporciona una rápida reducción del error del voltaje y por lo tanto, el mínimo error cuadrático (MSE). Por esta razón, el uso del convertidor VSC es considerado como la mejor estrategia para estabilizar el voltaje. Por otro lado, el mejor rango de voltajes es hayado en los nodos de las turbinas eólicas sólo en el caso en el que sus generadores son controlados como únicos dispositivos en la red. No obstante, dado que todos los nodos se encuentran dentro de sus respectivos rangos de seguridad, este último parámetro es considerado de menor importancia a la hora de decidir la mejor estrategia. Una vez se ha demostrado un exitoso comportamiento en la red del parque eólico, el controlador MPC integra un transformador OLTC externo. Dicha coordinación permite dos cosas.

Primero, mantener los nodos del parque en funcionamiento óptimo. Y en segundo lugar, mejorar el nivel del voltaje en un nodo externo conectado a una carga variable. Por lo tanto, esto justifica que un controlador MPC de un parque eólico puede coordinar eficazmente elementos de una red externa con el objetivo de mejorar ambas redes.

En conclusión, la técnica MPC funciona perfectamente para coordinación de elementos del sistema eléctrico. En este caso, el objetivo de minimizar la desviación del voltaje es conseguido con acciones de control óptimas juntando diferentes tecnologías. Las predicciones del controlador junto con una efectiva sensibilidad proporciona un excelente funcionamiento para los estudios llevados a cabo.

Bibliography

- [1] European Commission. *Energy Strategy and Energy Union*. 2015. URL: <https://ec.europa.eu/energy/en/topics/energy-strategy-and-energy-union/2020-energy-strategy>.
- [2] Danish Energy Agency. *Danish Climate Policies*. URL: <https://ens.dk/en/our-responsibilities/energy-climate-politics/danish-climate-policies>.
- [3] EWEA European Wind Energy Association. *Wind in power – 2015 European statistics*. 2016. URL: <http://www.eniscuola.net/en/mediateca/eu-power-mix-in-2000-and-in-2015>.
- [4] Wind Europe. *Wind in Power: 2016 European Statistics*. URL: <https://windeurope.org/about-wind/statistics/european/wind-in-power-2016/>.
- [5] State of Green. *Danish Energy Statistics 2015*. 2015. URL: <https://stateofgreen.com/en/profiles/danish-energy-agency/news/danish-energy-statistics-2015-renewables-now-cover-56-of-electricity-consumption>.
- [6] Danish Energy Agency. *Energy Statistics 2015*. 2015. URL: https://ens.dk/sites/ens.dk/files/Statistik/energy_statistics_2015.pdf.
- [7] Mattia Marinelli. *Enhancing the role of renewables in the grid*. 2016. Chapter 01 - Course 31783.
- [8] H. Zhao et al. “Coordinated Voltage Control of a Wind Farm Based on Model Predictive Control”. In: *IEEE Transactions on Sustainable Energy* 7.4 (October 2016), pages 1440–1451. ISSN: 1949-3029. DOI: 10.1109/TSTE.2016.2555398.
- [9] B.M. Weedy et al. *Electric Power Systems*. John Wiley & Sons Ltd, 2012. Chapter 2.5 - Power Transfer and Reactive Power.
- [10] Göran Andersson. *Dynamics and Control of Electric Power Systems*. ETH Zürich, 2012. Chapter 6 - Voltage Control in Power Systems.
- [11] M. Sarma J. Duncan and T. Overbye. *Power Systems Analysis and Design*. Cengage Learning, 2012. Chapter 12.1 - Generator-Voltage Control.
- [12] Jorge Martínez García. “Voltage Control in Wind Power Plants with Double Fed Generators”. PhD thesis. Alborg University, 2010. Chapter 2.3 - Plant Voltage Control.

- [13] Lennart Petersen and Fitim Kryezi. “Wind Power Plant Control Optimisation with Embedded Application of Wind Turbines and STATCOMs”. Alborg University, 2015. Chapter 2 - Wind Power Plant Reactive Power and Voltage Control Strategies.
- [14] L. Shi Q. Lu and N. Chen. “Study on Optimization Strategy for Voltage and Reactive Power Control of Wind Farm”. In: *International Conference on Applied Physics and Industrial Engineering - Elsevier* 24 (2012), pages 945–952.
- [15] T. Littler L. Meegahapola B. Fox and D. Flynn. “Multi-objective reactive power support from wind farms for network performance enhancement”. In: *International Transactions on Electrical Energy Systems* 23 (2013), pages 135–150.
- [16] Z. Xia Xing et al. “Multi-timescale multi-objective reactive power optimization of dispersed wind farm”. In: *Dianji Yu Kongzhi Xuebao/electric Machines and Control* 20.11 (2016), pages 46–52.
- [17] D. F. Opila, A. M. Zeynu, and I. A. Hiskens. “Wind farm reactive support and voltage control”. In: *2010 IREP Symposium Bulk Power System Dynamics and Control - VIII (IREP)*. August 2010, pages 1–10. DOI: 10.1109/IREP.2010.5563248.
- [18] D. Flynn L. Meegahapola S. Durairaj and B. Fox. “Coordinated utilisation of wind farm reactive power capability for system loss optimisation”. In: *European Transactions on Electrical Power* 21 (2011), pages 40–51.
- [19] Q. Wu et al. “Wind power plant voltage control optimization with embedded application of wind turbines and STATCOM”. In: *2016 Asian Conference on Energy, Power and Transportation Electrification (ACEPT)*. October 2016, pages 1–5. DOI: 10.1109/ACEPT.2016.7811534.
- [20] Qinglai Guo et al. “Hierarchical automatic voltage control for integration of large-scale wind power: Design and implementation”. In: *Electric Power Systems Research - Elsevier* 120 (2015), pages 234–241.
- [21] P. Thøgersen Z. Hussain Z. Chen and P. Lund. “Dynamic Reactive Power Compensation of Large-Scale Wind Integrated Power System”. In: *IEEE Transactions on Power Systems* 30.5 (2015), pages 2516–2526.
- [22] Z. Li J. Zhao and D. Li. “Reactive Power Optimization Algorithm of Considering Wind Farm Voltage Control Capability in Distribution System”. In: *International Conference on Electrical Machines and Systems, Icems* (2011).
- [23] J. J. Zhao et al. “Wind farm reactive power output optimization for loss reduction and voltage profile improvements”. In: *2009 IEEE 6th International Power Electronics and Motion Control Conference*. May 2009, pages 1099–1103. DOI: 10.1109/IPEMC.2009.5157548.
- [24] L. Papangelis et al. “Coordinated Supervisory Control of Multi-Terminal HVDC Grids: A Model Predictive Control Approach”. In: *IEEE Transactions on Power Systems* 32.6 (November 2017), pages 4673–4683. ISSN: 0885-8950. DOI: 10.1109/TPWRS.2017.2659781.

- [25] and T. Undeland T. M. Haileselassie M. Molinas. “Multi-Terminal VSC-HVDC System for Integration of Offshore Wind Farms and Green Electrification of Platforms in the North Sea”. In: 24 (). DOI: 10.1.1.630.6436.
- [26] Jizhong Zhu. *Optimization of Power System Operation*. John Wiley & Sons, Inc., 2009. Chapter 10.3 - Linear Programming Method of VAR Optimization.
- [27] Eduardo F. Camacho and Carlos Bordons. “Distributed model predictive control”. In: *Optimal Control Applications and Methods* 36 (2015), pages 269–271.
- [28] Yifei Guo et al. “Enhanced Voltage Control of VSC-HVDC Connected Offshore Wind Farms Based on Model Predictive Control”. In: *IEEE Transactions on Sustainable Energy* 9.1 (2018), pages 47–54.
- [29] Eduardo Camponogara and Helton F. Scherer. “Distributed Optimization for Model Predictive Control of Linear Dynamic Networks With Control-Input and Output Constraints”. In: *IEEE Transactions on Automation Science and Engineering* 8.1 (2011), pages 233–242.
- [30] K. Christakou et al. “Efficient Computation of Sensitivity Coefficients of Node Voltages and Line Currents in Unbalanced Radial Electrical Distribution Networks”. In: *IEEE Transactions on Smart Grid* 4.2 (June 2013), pages 741–750. ISSN: 1949-3053. DOI: 10.1109/TSG.2012.2221751.
- [31] M.H. Haque. “A general load flow method for distribution systems”. In: *Electric Power Systems Research - Elsevier* 54 (2000), pages 47–54.
- [32] Haoran Zhao et al. “Combined Active and Reactive Power Control of Wind Farms Based on Model Predictive Control”. In: *IEEE Transactions on Energy Conversion* 32.3 (2017), pages 47–54.
- [33] *Yalmip Toolbox*. 2015. URL: <https://yalmip.github.io/>.
- [34] Mosek Aps. *Mosek Solver*. 2015. URL: <https://www.mosek.com/>.
- [35] Christof Deckmyn et al. “A coordinated voltage control strategy for on-load tap changing transformers with the utilisation of distributed generators”. In: *IEEE International Energy Conference, Energycon* (2016).
- [36] F. Colas et al. J. Morin. “Embedding OLTC nonlinearities in predictive Volt Var Control for active distribution networks”. In: *Electric Power Systems Research - Elsevier* 143 (2017), pages 225–234.
- [37] ABB High Voltage Cable and ABB Power Systems. *HVDC Cable Transmissions*. URL: <https://library.e.abb.com/public/d4863a9b0f77b74ec1257b0c00552758/HVDC%20Cable%20Transmission.pdf>.
- [38] Dirk Van Hertem Jef Beerten and Ronnie Belmans. “VSC MTDC Systems with a Distributed DC Voltage Control – A Power Flow Approach”. In: *IEEE Trondheim PowerTech* (2011).
- [39] Song Ruihua et al. “VSCs based HVDC and its control strategy”. In: *IEEE/PES Transmission and Distribution Conference & Exhibition: Asia and Pacific, Dalian, China* (2005).

- [40] Mevludin Glavic Thierry Van Cutsem and William Rosehart. *IEEE PES Task Force on Test Systems for Voltage Stability Analysis and Security Assesment*. Technical report. 2015.
- [41] Francisco M. Gonzalez-Longatt and José Luis Rueda. *PowerFactory Applications for Power System Analysis*. 2014. Chapter Chapter 19 - Implementation of Simplified Models of Local Controller for Multi-terminal HVDC Systems in DIgSILENT PowerFactory.

Appendix A

Y_{bus} (1/p.u.)			
Branch: Bus $i - j$	Real Part	Imaginary Part	Absolute Value
Ext. - HV	-0,5124	2,8485	2,8942
HV - MV (OLTC)	-0,3200	19,9988	20,0014
MV - WT8 (Collector)	-5,2250	6,1114	8,04055
WT8 - WT9	-15,6751	18,3342	24,1216
WT9 - WT10	-15,6751	18,3342	24,1216

Table 1: Sample of Line Admittances of the WF

Bus Voltages (p.u.)			
Bus	Real Part	Imaginary Part	Absolute Value
Ext.	0,8423	-0,5358	0,9983
HV	0,6002	-0,7997	0,9999
MV	0,6375	-0,7709	1,0004
WT1	0,6790	-0,7731	1,0290
WT2	0,6909	-0,7738	1,0374
WT3	0,7007	-0,7745	1,0445
WT4	0,7086	-0,7751	1,0502
WT5	0,7145	-0,7755	1,0545
WT6	0,7184	-0,7758	1,0574
WT7	0,7204	-0,7759	1,0588
WT8	0,6551	-0,7720	1,0125
WT9	0,6589	-0,7722	1,0152
WT10	0,6607	-0,7725	1,0165
WT11	0,6665	-0,7715	1,0196
WT12	0,6742	-0,7716	1,0247
WT13	0,6803	-0,7716	1,0287
WT14	0,6843	-0,7716	1,0314
WT15	0,6863	-0,7717	1,0327
WT16	0,6662	-0,7712	1,0191
WT17	0,6738	-0,7712	1,0241
WT18	0,6793	-0,7713	1,0278
WT19	0,6828	-0,7713	1,0302
WT20	0,6843	-0,7714	1,0312

Table 2: Sample of Voltage Measurements at t_{70}

Voltage Magnitude Sensitivity to Q Injections (p.u. / MVAr)/(Base: 1×10^{-4})																							
Bus	MV	Ext	HV	1	2	3	4	5	6	7	8	9	10	11	12	13	14	15	16	17	18	19	20
MV	42	0	36	42	42	41	41	41	41	41	42	42	42	42	42	42	42	42	42	42	42	42	42
Ext.	0	0	0	0	0	0	0	0	0	0	0	0	0	0	0	0	0	0	0	0	0	0	0
HV	36	0	36	36	36	36	36	36	36	36	36	36	36	36	36	36	36	36	36	36	36	36	36
1	41	0	35	50	50	49	49	49	41	41	41	41	41	41	41	41	41	41	41	41	41	41	41
2	40	0	35	49	52	52	52	52	52	40	40	40	40	40	40	40	40	40	40	40	40	40	40
3	40	0	35	49	52	55	55	55	55	55	40	40	40	40	40	40	40	40	40	40	40	40	40
4	40	0	35	49	52	55	58	57	57	57	40	40	40	40	40	40	40	40	40	40	40	40	40
5	40	0	35	49	52	54	57	60	60	60	40	40	40	40	40	40	40	40	40	40	40	40	40
6	40	0	35	48	51	54	57	60	63	63	40	40	39	40	40	40	40	40	40	40	40	40	40
7	40	0	35	48	51	54	57	60	63	66	39	39	40	40	40	40	40	40	40	40	40	40	40
8	41	0	36	41	41	41	41	41	41	41	50	50	50	41	41	41	41	41	41	41	41	41	41
9	41	0	36	41	41	41	41	41	41	41	50	53	53	41	41	41	41	41	41	41	41	41	41
10	41	0	36	41	41	41	41	41	41	41	50	53	56	41	41	41	41	41	41	41	41	41	41
11	41	0	36	41	41	41	41	41	41	41	41	41	41	41	50	50	50	50	41	41	41	41	41
12	41	0	36	41	41	41	41	40	40	40	41	41	41	41	50	53	53	53	41	41	41	41	41
13	41	0	35	41	40	40	40	40	40	40	41	40	40	50	53	56	56	56	41	41	41	41	41
14	40	0	35	40	40	40	40	40	40	40	40	40	40	50	53	56	59	59	40	40	40	40	40
15	40	0	35	40	40	40	40	40	40	40	40	40	40	50	53	56	59	62	40	40	40	40	40
16	41	0	36	41	41	41	41	41	41	41	41	41	41	41	41	41	41	41	41	50	50	50	50
17	41	0	36	41	41	41	41	40	40	40	41	41	41	41	41	41	41	41	41	50	53	53	53
18	41	0	35	41	40	40	40	40	40	40	41	41	41	41	41	41	41	41	41	50	53	56	56
19	41	0	35	40	40	40	40	40	40	40	40	40	40	41	41	40	40	40	50	53	56	59	59
20	40	0	35	40	40	40	40	40	40	40	40	40	40	40	40	40	40	40	50	53	56	59	62

Table 3: Voltage Magnitude Sensitivity to Q Injections

Voltage Magnitude Sensitivity to $V_{HV}(p.u.)$			
Buses	Calculated Coefficients	Adjustment 1 For VSC Control	Adjustment 2 For OLTC Control
Ext.	0	0	0
HV	-1,2696	1	0
MV	-0,27099	0,2134	0,9987
WT1	-0,2643	0,2082	1,0053
WT2	-0,2623	0,2066	1,0073
WT3	-0,2606	0,2053	1,0090
WT4	-0,2593	0,2042	1,0103
WT5	-0,2582	0,2033	1,0114
WT6	-0,2575	0,2028	1,0121
WT7	-0,2572	0,2025	1,0124
WT8	-0,2678	0,2109	1,0018
WT9	-0,2671	0,2104	1,0025
WT10	-0,2668	0,2101	1,0028
WT11	-0,2662	0,2097	1,0034
WT12	-0,2649	0,2086	1,0047
WT13	-0,2639	0,2079	1,0057
WT14	-0,2632	0,2073	1,0063
WT15	-0,2629	0,2071	1,0067
WT16	-0,2663	0,2097	1,0033
WT17	-0,2651	0,2087	1,0045
WT18	-0,2641	0,2080	1,0055
WT19	-0,2635	0,2075	1,0061
WT20	-0,2633	0,2073	1,0063

Table 4: Voltage Magnitude Sensitivity to V_{POC}

Appendix B

```
1  %-----  
2  % Definition of buses  
3  slack_Bus = 2;  
4  hv_Bus = 3;  
5  mv_Bus = 1;  
6  
7  % Voltage measurements  
8  v_vec_full=v_vec;  
9  Vcomplex = v_vec;  
10 Vmag = abs(Vcomplex);  
11  
12 % Admittances: Ybus  
13 %Y_matrix = Ybus; --> Change format of Ybus into matrix  
14 [I,J,s] = find(Ybus);  
15 for m=1:size(I,1)  
16     Y_matrix(I(m),J(m)) = s(m);  
17 end  
18  
19 %%  
20 %-----  
21 % Sensitivity calculation  
22 %-----  
23 % Generate parameters of Equations (2.5) and (2.10)  
24 % Parameters: Summatory of relationship between Ybus and Voltages  
25 % Unknowns: Partial derivatives  
26  
27 % Development of parameters  
28 % Assumption 1: Derivative of conjugate is conjugate of derivative  
29 % Assumption 2: Cauchy-Riemann Equations: Derivative=[a -b; b a]  
30 % Partial derivatives like common factor  
31  
32 % A_mat = Summatory of the first part of the equation  
33 % B_mat = Summatory of the second part of the equation  
34 % D_mat = Sum of A_mat and B_mat  
35 % D_mat = [A_real+B_real    -(-A_im+B_im);  
36            A_iml+B_im      -A_real+B_real];  
37 % Formulate D_mat  
38 A_mat=zeros(size(Ybus,1),size(Ybus,1));  
39 for n=1:1:size(Ybus,1)  
40     A_mat(n,n)=Ybus(n,:)*v_vec;  
41 end  
42 B_mat=zeros(size(Ybus,1),size(Ybus,1));  
43 for n=1:1:size(Ybus,1)
```

```

43     B_mat(n,:)=conj(v_vec(n))*Ybus(n,:);
44     end
45     D_mat11=real(A_mat+B_mat);
46     D_mat12=real(-A_mat*1i+B_mat*1i);
47     D_mat21=imag(A_mat+B_mat);
48     D_mat22=imag(-A_mat*1i+B_mat*1i);
49
50     % Remove external network bus: slack_Bus
51     D_mat11(slack_Bus,:)=[];
52     D_mat11(:,slack_Bus)=[];
53
54     D_mat12(slack_Bus,:)=[];
55     D_mat12(:,slack_Bus)=[];
56
57     D_mat21(slack_Bus,:)=[];
58     D_mat21(:,slack_Bus)=[];
59
60     D_mat22(slack_Bus,:)=[];
61     D_mat22(:,slack_Bus)=[];
62
63     D_mat = [D_mat11, D_mat12;
64             D_mat21, D_mat22];
65     NUM = D_mat;
66
67     v_vec(slack_Bus,:)=[];
68
69     Y_matrix(slack_Bus,:) = [];
70     Y_matrix(:,slack_Bus) = [];
71
72     %-----
73     % Q sensitivity
74     %-----
75
76     Qsen_mat=zeros(size(Ybus,1),size(Ybus,1));
77     for inj_Bus=1:size(Ybus,1)
78         C_mat=zeros(size(Ybus,1),1);
79         for n=1:1:size(Ybus,1)
80             % Generate results of Equation (2.5)
81             if n==inj_Bus
82                 C_mat(n,1)=-1; % If i=1 -> Solution = -j1
83             end
84         end
85         C_mat(slack_Bus,:)=[];
86         E_mat = [0*C_mat;C_mat]; %Split into real and imaginary part:
87                 % [real=0; imag=-1j]
88         res_vec=inv(D_mat)*E_mat; %Solve system of equations
89
90         Qsen_vec=zeros(size(Ybus,1)-1,1);
91         for n=1:1:size(Ybus,1)-1
92             Qsen_vec(n)=1/abs(v_vec(n))*real(conj(v_vec(n))*(res_vec(n)+1i*(
93             res_vec(n+size(Ybus,1)-1)))/Sbase;
94         end
95
96         %Include Slack bus
97         if slack_Bus==1

```

```

97     Qsen_vec=[0;Qsen_vec];
98     elseif slack_Bus==size(Ybus,1)
99         Qsen_vec=[Qsen_vec;0];
100     else
101         Qsen_vec=[Qsen_vec(1:slack_Bus-1);0;Qsen_vec(slack_Bus:end)];
102     end
103     Qsen_mat(:,inj_Bus)=Qsen_vec;
104 end
105 % Final Results: Qsen_mat
106
107 %-----
108 %Voltage sensitivity of bus 'i' to slack bus 'k'
109 %-----
110
111 dVimagdVk = zeros(size(Ybus,1)-1, 1);
112 k = 2; % k= POC bus = HV bus --> k=2 after removing Slack_Bus
113 N = size(Ybus,1) - 1;
114 M = size(Ybus,1);
115
116 % Create results of equation (2.10)
117 RES_dVidVk = zeros(2*N, 1); % Real and Imag part of
118     each N bus
119 theta = angle(Vcomplex(k));
120 for m=1:1:N
121     RES_dVidVk(m, 1) = real( (-1) * conj(Vcomplex(m)) * Y_matrix(m,
122     k) * (cos(theta) + sin(theta)*1i));
123     RES_dVidVk(m+N, 1) = imag( (-1) * conj(Vcomplex(m)) * Y_matrix(m
124     , k) * (cos(theta) + sin(theta)*1i));
125 end
126
127 % Solve system of equations
128 XY_Wik = inv(NUM) * RES_dVidVk;
129
130 % Find out results of each partial derivative
131 for n=1:N % n = states subindex of
132     Vi (denominator)
133     dVidVk(n, 1) = XY_Wik(n) + XY_Wik(n+N)*i;
134     dVimagdVk(n, 1) = real( dVidVk(n, 1) / Vcomplex(n)) * Vmag(n);
135 % Equation (2.12)
136     dViargdVk(n, 1) = imag( dVidVk(n, 1)) / Vcomplex(n) ;
137 end
138 % Final Results: dVimagdVk
139
140 % ADJUSTMENT 1
141 dVimagdVk_1 = dVimagdVk / (dVimagdVk(k)); % Get Unity ratio
142 dVimagdVk_1 = [dVimagdVk_1(1); 0; dVimagdVk_1(2:end)]; % Include Slack
143     bus
144
145 %-----
146 %Voltage sensitivity of bus 'i' to N_TAP step
147 %-----
148 % ADJUSTMENT 2

```

```
146 dVimagdVk_2 = dVimagdVk + -1*(dVimagdVk(k)); % Strong external influence
147 dVimagdVk_2 = [dVimagdVk_2(1); 0; dVimagdVk_2(2:end)]; % Include Slack
    bus
148
149 % Tap changer sensitivity
150 tap_voltage = 0.0125;
151 dVtap = tap_voltage;
152 for n=1:M
153     dVimagdNtap(n, 1) = dVimagdVk_2(n, 1) * dVtap;
154     % Delta in this case means an increment instead of the derivative
155 end
```

Sensitivity_coefficients_calculation.m

